Programming Quantum Circuit Parameters with Large Language Models

Farias, T.S.,[1,2,*] Porto, C.M.,[2] Fonseca, M. S.,[2] Carpio, N. A. C.,[2] De Oliveira, A. A.,[2] and Villas-Boas, C. J[2]

[1] *University of Innsbruck, Department of Physics, Technikerstrasse 25, 6020 Innsbruck, Austria*
[2] *Federal University of São Carlos, Department of Computer Science, Rod. Washington Luís, km 235, Jardim Guanabara, São Carlos - SP, 13565-905, Brazil*

Large language models (LLMs) have recently demonstrated the ability to generate parameters for variational quantum circuits without conventional optimization. However, the conditions under which this approach is effective remain unclear. Here, we investigate a frozen, general-purpose LLM that generates complete circuit parameter vectors from symbolic circuit and Hamiltonian descriptions, with optional iterative energy feedback. We evaluate the approach on general random Hamiltonians, structured parent Hamiltonians, and molecular systems. For general Hamiltonians, LLM-generated parameters exhibit larger energy errors than conventional Adam optimization, while additional feedback generally provides limited improvement. In contrast, for structured Hamiltonians, the LLM can generate promising low-energy parameter configurations, suggesting that identifiable physical and mathematical structure facilitates parameter inference. We also show that direct LLM predictions of minimum energies can violate the Hamiltonian spectral lower bound, whereas generated circuit parameters allow independent evaluation of physically realizable energy expectation values. Finally, we investigate blind circuit interpretation and find that the LLM can predict measurement outcomes even when it fails to identify the underlying quantum algorithm. These findings highlight the role of problem structure, the limitations of iterative LLM optimization, and the importance of independently verifiable predictions in quantum parameter programming.

arXiv:2611.17246v1 [quant-ph] 12 Nov 2026

I. INTRODUCTION

Variational quantum algorithms (VQAs) combine parameterized quantum circuits with classical optimization to address computational problems in quantum simulation, optimization, and machine learning [1, 2]. In this framework, a quantum processor prepares a state using a set of trainable circuit parameters, while a classical optimizer updates these parameters based on evaluations of an objective function. The variational quantum eigensolver (VQE), for example, seeks to minimize the expectation value of a Hamiltonian to approximate its ground-state energy. Although this hybrid approach can accommodate the constraints of current quantum devices, its practical performance depends on both the quality of the parameterized circuit and the efficiency of the optimization procedure.

A central challenge is the number of quantum circuit evaluations required during optimization. When the objective function is estimated on quantum hardware, each evaluation involves circuit executions and measurements, potentially across multiple Pauli terms of the Hamiltonian. Gradient-based approaches introduce additional evaluations to estimate derivatives. For example, the parameter-shift rule commonly requires two shifted expectation evaluations per independently parameterized rotation [3]. As the number of parameters grows, the measurement demands can become substantial, while statistical fluctuations and unfavorable optimization landscapes may further complicate convergence [4]. Consequently, reducing the number of quantum objective evaluations needed to identify useful circuit parameters is an important consideration in variational quantum optimization.

Neural networks have been investigated as a means of learning optimization strategies rather than relying exclusively on predefined update rules. Andrychowicz et al. [5] introduced a learning-to-optimize framework in which recurrent neural networks learn parameter updates across optimization tasks. Subsequent studies examined the scalability, generalization, and computational trade-offs of learned optimizers [6–8]. Unlike conventional optimizers with fixed update procedures, these approaches acquire optimization behavior through training on previous tasks. Their application to new problems therefore generally depends on specialized meta-training. Recent work has additionally examined reactive optimization rules that respond to local optimization information [9]. Such methods provide a useful point of comparison for distinguishing inference-time parameter generation from learned update mechanisms.

Related approaches have been developed for parameterized quantum circuits. Verdon et al. [10] trained classical recurrent neural networks to propose useful parameters for variational quantum algorithms, including QAOA and VQE. Khairy et al. [11] investigated learning-based strategies for optimizing variational quantum circuits in combinatorial problems, while Friedrich and Maziero [12] combined neural optimization with evolutionary strategies. More recently,

* tiago.farias@ufscar.br

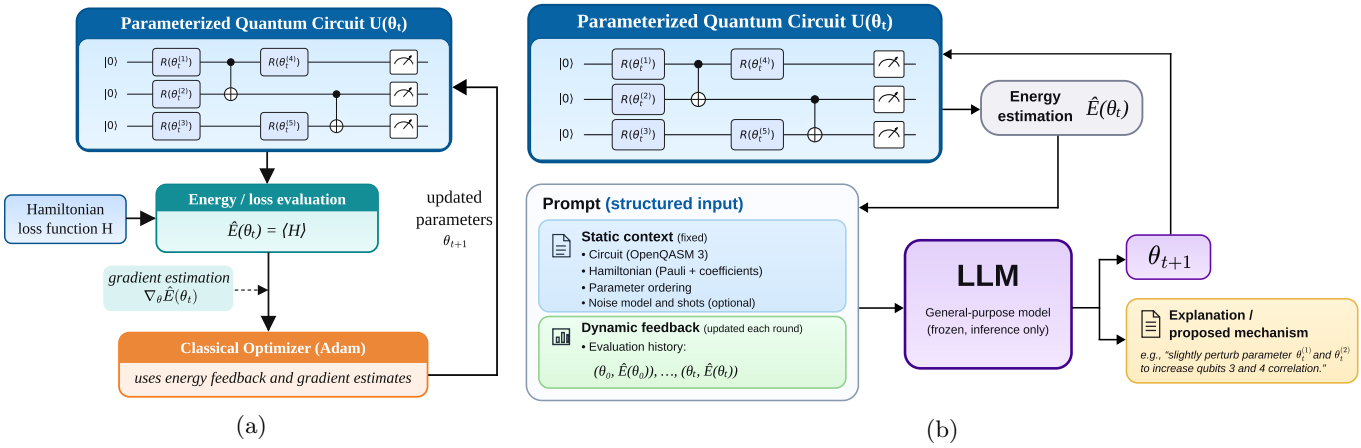


Figure 1: Comparison of conventional gradient-based variational optimization and language model optimizer. (a) A classical optimizer updates circuit parameters using quantum objective evaluations and parameter-shift gradient estimates. (b) A frozen large language model receives a symbolic description of the parameterized circuit and Hamiltonian and proposes a complete parameter vector without initial objective feedback. Subsequent proposals may incorporate previously evaluated parameters and their measured energies. Both approaches use the same parameterized quantum circuit; they differ in how candidate parameters are generated.

Zou et al. [13] introduced Flow-VQE, which learns a generative distribution of low-energy circuit parameters through energy-based preference training. These studies show that learned parameter generation can reduce optimization demands, although the resulting models depend on dedicated training procedures. Other relevant directions include meta-learning across quantum optimization tasks [14], learning quantum optimization strategies with quantum neural networks [15], and parameter transfer between QAOA problems using graph structure or symmetries [16, 17]. Parameter initialization can itself affect trainability, as investigated through reduced-domain initialization [18]. These studies motivate comparing the Language Model Optimizer (LMO) not only against generic numerical optimization but also against structure-aware initialization and transfer strategies.

Large language models have also emerged as general-purpose optimization agents. Yang et al. [19] introduced Optimization by Prompting, in which an LLM proposes candidate solutions using previously evaluated candidates and their objective values. Huang et al. [20] subsequently investigated the capabilities and limitations of LLMs for numerical black-box optimization. These approaches motivate the use of language models as optimization agents, but objective feedback remains an important source of problem-specific information during the search process. A broader survey places LLM-based optimization within classical and evolutionary optimization methods [21], while SemanticOpt explicitly investigates semantic information in black-box optimization [22]. Beyond proposing candidate solutions, LLMs have also been investigated for direct parameter generation. Wang et al. [23] explored neural-network parameter generation using LLMs trained on network checkpoints and task-specific descriptions.

A related and emerging direction is Weight-Space Programming, in which language models directly inspect, generate, or modify model parameters. Takehi et al. [24] presented preliminary evidence that a general-purpose LLM can interpret and edit neural-network weights directly, without conventional gradient-based training or a separately trained optimizer. Unlike approaches that learn parameter-update rules, this perspective involves operating directly on parameter values, potentially exploiting structural information about the model and its intended behavior. We note that, in parallel with the preparation of this work, Kundu et al. [25] independently investigated direct parameter generation for variational quantum circuits using general-purpose language models. Their study considered VQE, QAOA, and quantum classification, emphasizing parameter quality and initialization for classical optimization. While both works investigate parameter generation without task-specific training, our study additionally examines iterative energy feedback, performance across structured and general Hamiltonians, the physical verifiability of energy predictions, and blind quantum circuit interpretation.

In quantum computing, language models have also been investigated for circuit generation and parameter initialization. Jern et al. [26] introduced Agent-Q, which uses fine-tuned LLMs to generate parameterized quantum circuits. Zhuang and Guan [27] proposed AdaInit, which uses LLM-generated initial parameters and gradient feedback to improve the trainability of quantum neural networks. Macarone-Palmieri and Lo Franco [28] investigated iterative circuit synthesis using simulation feedback. These studies demonstrate the potential of LLMs for quantum circuit generation, parameter initialization, and iterative optimization. The present work focuses specifically on generating complete parameter vectors for a fixed circuit directly from its symbolic representation and target Hamiltonian,

without task-specific model training or initial objective-function feedback. Additional work explores LLM-assisted QAOA circuit generation [29], autonomous variational circuit design [30], and LLM-generated circuits and initialization designed to address trainability [31]. These circuit-design tasks differ from the present setting, where the circuit architecture remains fixed and the LMO returns its numerical parameters.

Recent evidence that general-purpose LLMs can directly generate parameters for variational quantum circuits motivates further investigation of the conditions under which this capability is effective. In particular, it remains important to understand how parameter generation depends on the structure of the circuit and Hamiltonian, and whether limited objective-function feedback can improve subsequent proposals. A quantum circuit specifies the order and action of its gates, while the Hamiltonian defines the energy to be minimized. Together, these descriptions provide problem-specific information that may guide parameter generation independently of previously measured objective values.

In this work, we investigate a Language Model Optimizer (LMO) that generates numerical parameters for fixed quantum circuits, as illustrated in Fig. 1. The approach uses a frozen, general-purpose LLM that receives the parameterized circuit in OpenQASM 3 [32] and the Hamiltonian as a Pauli decomposition. Without task-specific training or previous objective evaluations for the given instance, the model proposes a complete parameter vector. The resulting circuit is then evaluated, and subsequent proposals may incorporate previously tested parameters and their measured energies. This separates parameter generation from quantum evaluation and permits symbolic inference to precede measurement-based optimization.

This distinction is particularly relevant when quantum objective evaluations are expensive. The LMO generates its initial parameter vector without receiving any prior energy evaluations. The proposed parameters can then be evaluated through a single Hamiltonian expectation-value estimation to assess their quality. Depending on the experimental protocol, the resulting energy may be returned to the model as feedback for subsequent proposals or used solely for independent evaluation. The use of iterative feedback is specified separately for each experiment. However, generating parameters without initial objective feedback does not remove the need for experimental validation, nor does it imply that the proposed parameters are optimal for arbitrary Hamiltonians. Moreover, the cost of LLM inference must be distinguished from the number of quantum objective evaluations. The present approach therefore investigates a different information-resource trade-off rather than establishing a general computational advantage over classical optimization.

We evaluate the LMO across general random Hamiltonians, structured parent Hamiltonians with known ground-state energies, and molecular systems. These benchmarks allow us to investigate the quality of initial parameter proposals, the influence of problem structure, the effect of iterative energy feedback, and the number of objective evaluations required relative to conventional optimization. We also examine direct LLM predictions of minimum energies, distinguishing numerical estimates from physically realizable and independently verifiable parameter configurations. Beyond optimization, we investigate the ability of the same general-purpose model to interpret quantum circuits from their symbolic representations, distinguishing algorithm identification from functional output prediction. Together, these experiments characterize the capabilities and limitations of inference-time quantum parameter programming across different problem settings.

II. LANGUAGE MODEL-BASED QUANTUM CIRCUIT ANALYSIS

We investigate two complementary capabilities of a frozen, general-purpose large language model: circuit optimization and circuit interpretability. The first examines whether the model can generate numerical parameters that minimize the energy expectation value of a fixed quantum circuit. The second evaluates its ability to infer the computational behavior and possible purpose of quantum circuits directly from their symbolic representations, without executing them.

A. Circuit optimization

We consider the optimization of a fixed parameterized quantum circuit $U(\boldsymbol{\theta})$ acting on an n-qubit initial state $|0\rangle^{\otimes n}$, where $\boldsymbol{\theta} \in \mathbb{R}^p$ denotes the vector of p adjustable parameters. The prepared state and its energy expectation value are defined as

$$|\psi(\boldsymbol{\theta})\rangle = U(\boldsymbol{\theta})\,|0\rangle^{\otimes n}\,, \qquad E(\boldsymbol{\theta}) = \langle\psi(\boldsymbol{\theta})|\,H\,|\psi(\boldsymbol{\theta})\rangle\,. \tag{1}$$

For a Hamiltonian expressed as a linear combination of Pauli operators,

$$H = \sum_{j=1}^{M} c_j P_j, \qquad E(\boldsymbol{\theta}) = \sum_{j=1}^{M} c_j \langle P_j \rangle_{\boldsymbol{\theta}}, \tag{2}$$

where $c_j \in \mathbb{R}$ and $P_j \in \{I, X, Y, Z\}^{\otimes n}$. The objective is to find a parameter vector that minimizes $E(\boldsymbol{\theta})$. On quantum hardware, the energy is estimated from finite measurement samples, yielding an estimator $\widehat{E}(\boldsymbol{\theta})$.

Motivated by the weight-space programming perspective [24], the LMO treats circuit parameters as numerical quantities that can be directly inferred and modified by a language model, rather than exclusively updated through conventional optimization rules. We employ a frozen, general-purpose LLM to propose complete parameter vectors from a symbolic description of the parameterized circuit in OpenQASM 3 and the Hamiltonian specified by its Pauli operators and coefficients. The same system instructions are used across all benchmark instances. They specify the energy-minimization objective, the Pauli-label ordering convention, and the required output format. The LMO is not provided with the hidden generating parameters, known ground-state energy, target state, classical optimization trajectories, or numerical statevectors. No task-specific training or parameter updates are performed on the language model. Let $\mathcal{C}$ denote the parameterized OpenQASM 3 description, $\mathcal{H} = \{(c_j, P_j)\}_{j=1}^{M}$ the Hamiltonian representation, and $\mathcal{N}$ any optional disclosed information. Before receiving objective-value feedback, the first proposal is generated as

$$\boldsymbol{\theta}_1 = \mathcal{R}_{\mathrm{LMO}}\left(\mathcal{C}, \mathcal{H}, \mathcal{N}\right), \tag{3}$$

where $\mathcal{R}_{\mathrm{LMO}}$ represents the language-model inference procedure. The proposed vector is evaluated only after generation, so the initial proposal does not depend on quantum objective evaluations performed for that instance. After the initial evaluation, the LMO may refine its proposals using the history of previously evaluated parameter vectors and their corresponding energy estimates. This iterative use of objective-value feedback is related to LLM-based optimization approaches such as Optimization by Prompting [19]. The feedback history is defined as

$$\mathcal{F}_t = \left\{ \left(\boldsymbol{\theta}_i, \widehat{E}_i \right) \right\}_{i=1}^{t}. \tag{4}$$

Each inference produces one complete numerical parameter vector, rather than an individual coordinate update. The model also returns a textual explanation of its proposed modification, but this explanation is not used to evaluate or accept the candidate. The optimization feedback consists of the numerical energy estimate obtained from the corresponding circuit evaluation. To assess the use of quantum resources, we distinguish Hamiltonian expectation-value evaluations. Each evaluated LMO proposal requires one complete Hamiltonian expectation-value evaluation to obtain objective feedback, irrespective of the number of circuit parameters. For a Hamiltonian containing multiple Pauli terms, a complete evaluation may require measurements in several bases and repeated circuit executions. In the simulations presented in this work, we count complete energy evaluations without assigning a physical measurement-shot cost.

B. Circuit interpretability

Beyond generating circuit parameters, we investigate whether a general-purpose large language model can infer the computational behavior of quantum circuits from their symbolic representations without executing them. Related studies have investigated the interpretation of computational models from their internal representations. Kabra et al. [33] developed Weight Oracles, using specialized language models to infer properties of neural networks directly from their weights. In quantum computing, Chen et al. [34] investigated symbolic interpretation of Grover circuits using a domain-adapted language model. More recently, Mondal [35] introduced QuantumSemEval, a benchmark evaluating whether LLMs can recognize semantic equivalence between structurally different quantum programs. Related work includes GroverGPT, a language model focused on quantum search [36], and benchmarks of quantum-computing reasoning [37] and quantum-code generation evaluation [38]. Broader perspectives on artificial intelligence for quantum computing are also available [39]. Together, these works motivate evaluating functional predictions separately from algorithm-label recognition.

Here, we investigate whether a frozen, general-purpose LLM can infer the computational behavior of individual quantum circuits under semantics-preserving changes in representation. Unlike pairwise equivalence checking, our protocol evaluates each representation independently and distinguishes algorithm identification from functional output prediction.

We formulate this task as blind circuit interpretation. Given a circuit represented in OpenQASM 3, the frozen LLM is asked to describe its mathematical behavior, identify its possible computational purpose, and predict observable outcomes when these can be determined, as illustrated in Fig. 2. The input includes the gate operations, numerical parameters, qubit interactions, and measurement instructions, but excludes the algorithm name, expected solution, and benchmark metadata. The model receives no statevectors, simulated measurements, or experimental feedback.

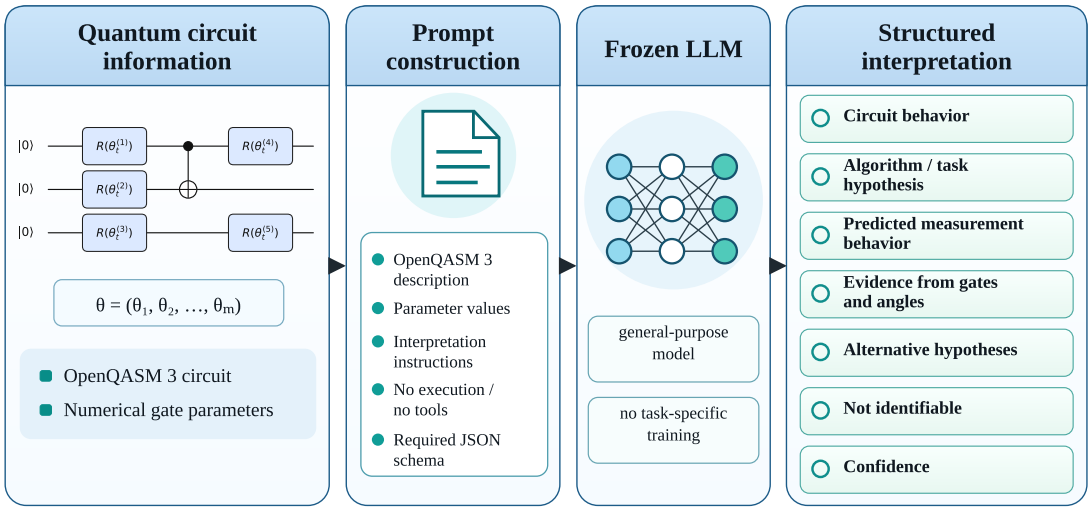


Figure 2: Blind interpretation of quantum circuits using a frozen large language model. A circuit and its numerical parameters are serialized into OpenQASM 3 and provided without algorithm-specific metadata. The model generates a structured interpretation describing the circuit behavior, possible computational purpose, expected measurement outcomes, supporting gate-level evidence, alternative hypotheses, and uncertainty. Its predictions are subsequently compared with independently established circuit properties.

We consider three quantum algorithms with distinct computational behaviors: Grover's search algorithm, the quantum Fourier transform (QFT), and the Bernstein-Vazirani algorithm. For each algorithm, we construct five instances with different problem parameters or input states. Each instance is expressed in three representations: logical, using standard quantum gates; native, obtained by decomposition into the restricted gate basis $\{R_Z, R, R_{XX}\}$; and obfuscated, obtained through randomized local Clifford-frame transformations followed by native-gate decomposition. The transformations preserve the implemented computation, which is verified numerically before inference.

The three representations allow us to investigate whether the model's interpretation depends on familiar gate sequences. Logical circuits retain recognizable algorithmic structures, whereas native decomposition and randomized frame transformations modify their gate-level descriptions. Algorithm-specific identifiers and comments are removed from all representations. The resulting circuit descriptions are evaluated independently, without providing the model with their equivalence relationships.

For every circuit, the LLM receives the same instructions and returns a structured response containing its inferred circuit behavior, algorithm hypothesis, predicted measurement behavior, supporting evidence, alternative hypotheses, and uncertainty. When a specific output bitstring can be inferred, the model may report that prediction explicitly, otherwise, it may abstain. No external tools, simulations, or circuit executions are available to the model during inference. The ground-truth circuit properties are determined independently and are not included in the model input. The different representations preserve the underlying computation but may differ in circuit depth and description length. Consequently, this protocol evaluates robustness under representation changes rather than isolating the effect of obfuscation alone. Correct interpretation of transformed circuits does not, by itself, rule out the use of patterns learned during language-model training. Further implementation details and evaluation criteria are provided in Appendix I.

III. RESULTS

This section presents the experimental evaluation of the LMO across parameter optimization, iterative feedback, and circuit interpretation. For parameter optimization, we consider two families of problems: general Hamiltonians and structured Hamiltonians, including parent and molecular Hamiltonians. The results support four main observations:

- **General Hamiltonians.** For general Hamiltonians, the LLM struggles to identify low-energy parameter configurations and does not consistently outperform conventional optimization with Adam.
- **Structured Hamiltonians.** For Hamiltonians with identifiable physical or mathematical structure, such as parent and molecular Hamiltonians, the LLM can generate promising parameter configurations, suggesting that problem-specific structure may facilitate parameter inference. In some molecular experiments, successive LMO proposals yield further reductions in energy, although the contribution of energy feedback cannot be isolated from the effect of generating additional proposals.
- **Iterative feedback.** Successive LMO proposals generally provide limited improvement over the initial parameter configuration, although substantial energy reductions are observed in some molecular experiments. Since additional proposals are generated alongside the incorporation of previous energy evaluations, the specific contribution of feedback remains undetermined.
- **Circuit interpretability.** The LLM can identify certain quantum algorithms from their circuit representations, including some obfuscated circuits. Even when algorithm identification fails, the model can sometimes correctly predict the most likely measurement bitstring.

All LLM-based experiments reported in this work use GPT-6 Astra. For experiments involving the Adam optimizer [40], we performed a preliminary learning-rate search over $\{10^0, 10^{-1}, 10^{-2}\}$. The learning rate yielding the lowest final energy under a fixed optimization budget was selected for the subsequent experiments.

A. Circuit optimization

We evaluate the LMO on three classes of optimization problems: molecular Hamiltonians, general random Hamiltonians, and structured parent Hamiltonians. These problems differ in their physical interpretation and mathematical structure, allowing us to investigate how these properties influence the quality of LLM-generated circuit parameters. For each problem, we examine the initial parameter proposals, the effect of iterative energy feedback, and their performance relative to conventional optimization with Adam.

1. H_4 Molecule

We investigate the LMO on the molecular ground-state energy problem of H_4, considering a fixed planar molecular geometry described using the STO-3G basis. The system contains four electrons distributed over four spatial orbitals, without additional active-space truncation, generating a total of 8 spin-orbital, the same as the number of qubits. As illustrated in Fig. 3, the molecular system is represented by a qubit Hamiltonian which generates a fixed UCCSD[41] parameterized quantum circuit. These representations are provided to the LMO, which proposes complete parameter vectors together with a textual explanation of the proposed mechanism. The generated parameters are used to instantiate the circuit, whose energy expectation value is evaluated and may be incorporated into subsequent proposals. Details of Hamiltonian construction and the circuit ansatz are provided in Appendix B. The molecular coordinates and additional H_4 results are given in Appendix D.

We consider two prompting strategies. In the blind configuration, the LMO receives the parameterized circuit description and the Hamiltonian as a Pauli decomposition, without additional chemical information. In the physics-aware configuration, the same inputs are supplemented with molecular information, including the geometry, basis set, electronic configuration, active space, and reference state, as indicated by the dashed arrow in Fig. 3. The standard optimization instructions and parameter-output format are preserved, with the physics-aware instructions additionally allowing the use of chemical context. Both configurations use the same frozen language model and circuit architecture. The corresponding prompts are documented in Appendix A.

To examine the variability of the generated parameters, each prompting configuration is evaluated in three independent runs using the same initial prompt and language model. Within each run, the LMO may incorporate previously evaluated parameter vectors and their corresponding energies to generate subsequent proposals. We compare the resulting optimization trajectories with those of the gradient-based Adam optimizer. Performance is measured by the energy error relative to the active-space full configuration interaction (FCI) reference, expressed as a function of the cumulative number of Hamiltonian energy evaluations.

Figure 4 presents the optimization trajectories for the standard planar geometry. The physics-aware prompt produces the lowest energy errors, with some runs approaching the reference energy after only a few evaluations. Several physics-aware trajectories show further energy reductions across successive proposals, whereas the blind configurations

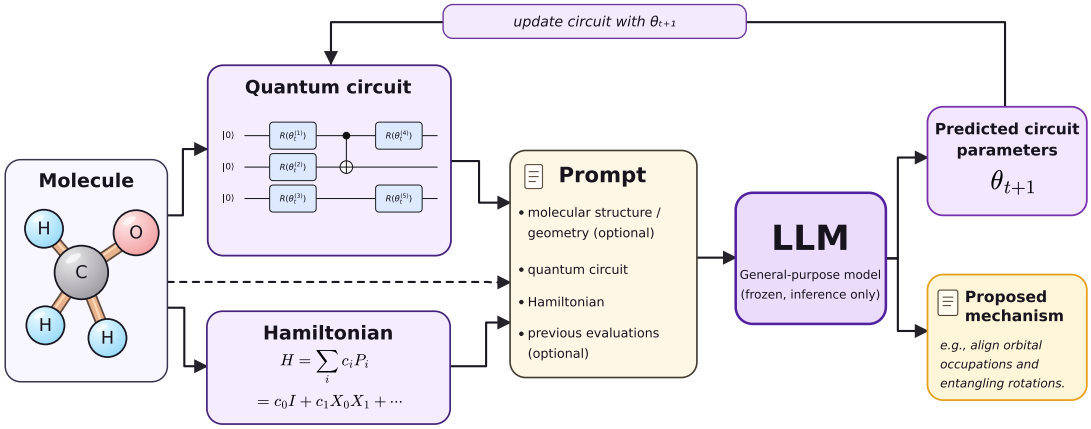


Figure 3: Workflow of language-model-based parameter optimization for molecular Hamiltonians. A molecular system is represented by a qubit Hamiltonian and a fixed parameterized quantum circuit. Their symbolic descriptions are incorporated into a prompt, optionally supplemented with molecular information and previous energy evaluations. A frozen, general-purpose LLM generates a complete parameter vector and a textual explanation of its proposed mechanism. The predicted parameters are assigned to the circuit, which can subsequently be evaluated to provide energy feedback for further proposals. Solid arrows indicate the main information and parameter flow, while the dashed arrow represents optional molecular information supplied directly to the prompt.

exhibit comparatively limited improvement. These observations suggest that additional molecular information may facilitate the generation of effective parameter configurations. However, the contribution of energy feedback cannot be isolated from that of generating additional candidate parameters, and performance varies across independent runs. Adam follows a more gradual optimization trajectory, continuing to reduce the energy error over a substantially larger evaluation budget. The comparison concerns Hamiltonian expectation-value evaluations rather than the total computational cost of LLM inference.

To probe generalization beyond the standard geometry, we also evaluate a distorted, nonplanar H_4 structure with modified Hamiltonian coefficients. Its coordinates, motivation, and optimization trajectories are reported in Appendix D.

2. *Random Hamiltonians*

We consider a family of randomly generated Hamiltonians to evaluate the ability of the LMO to identify low-energy circuit parameters in the absence of an explicitly structured physical problem. Each Hamiltonian is defined as

$$H = \sum_{j=1}^{M} c_j P_j, \qquad P_j \in \{I, X, Y, Z\}^{\otimes n}, \tag{5}$$

where M is the number of Pauli terms, n is the number of qubits, and the coefficients are independently sampled from

$$c_j \sim \mathcal{N}\left(0, \frac{1}{M}\right). \tag{6}$$

Each Pauli string contains exactly three non-identity operators, selected from $\{X, Y, Z\}$ and assigned to distinct qubit positions. Duplicate strings are excluded, and each generated Hamiltonian is required to contain at least one pair of anticommuting Pauli terms.

We investigate systems with $n \in \{4, 8, 12\}$ qubits, using a fixed ansatz with $L = n$ entangling layers. Each rotation block applies R_X, R_Y, and R_Z gates to every qubit, followed by a brickwork arrangement of CNOT gates connecting nearest-neighbor qubits. The entangling layers alternate between even and odd neighboring pairs, with an additional rotation block at the end of the circuit. The resulting ansatz contains $p = 3n(L + 1)$ trainable parameters. For each system size, we generate five independent Hamiltonian instances, each containing $M = 16$ Pauli terms.

We compare three approaches on the same Hamiltonian instances and circuit architectures. First, Adam optimizes randomly initialized circuit parameters using parameter-shift gradients. Second, the LMO generates complete



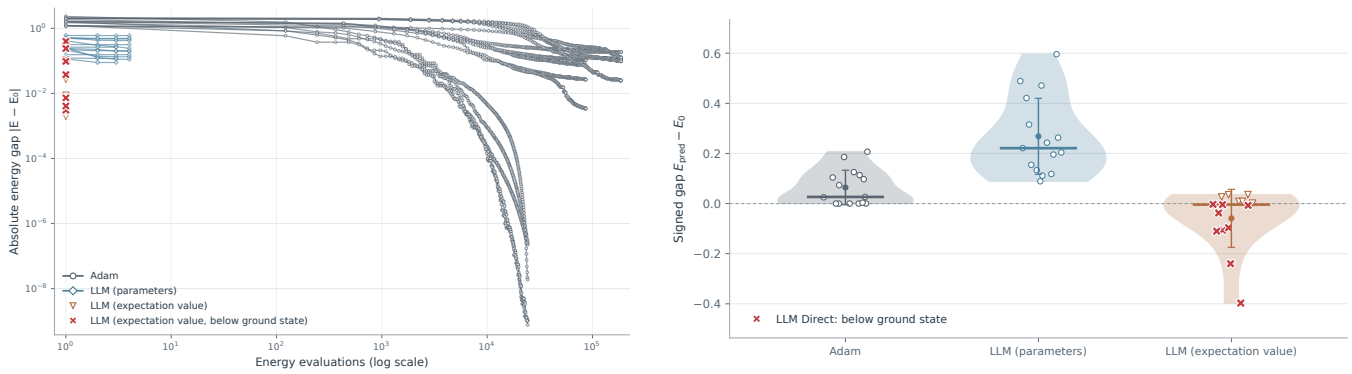
Figure 4: Optimization of the H_4 molecular Hamiltonian at the standard planar geometry,using Adam and the language model optimizer. The LMO is evaluated with a standard blind prompt and a physics-aware prompt containing additional chemical information, denoted as standard and chemical, respectively. Three independent runs are shown for each prompting configuration. The vertical axis represents the energy error relative to the active-space full configuration interaction reference, while the horizontal axis shows the cumulative number of Hamiltonian energy evaluations on a logarithmic scale. The dashed horizontal line indicates the chemical-accuracy threshold of 1 kcal/mol. The upper horizontal axis indicates the corresponding Adam optimization iterations.

parameter vectors from the circuit description and the Hamiltonian expressed as Pauli operators and coefficients. Subsequent LMO proposals may incorporate previously evaluated parameters and their energy expectation values as feedback. Third, we investigate direct energy prediction, in which the LLM estimates the minimum energy attainable by the fixed parameterized circuit without generating or evaluating a parameter vector. Unlike Adam and the LMO, this approach does not prepare a quantum state and therefore does not produce a variational energy estimate. Consequently, its predicted energy may fall below the true Hamiltonian ground-state energy.

All circuit energy expectation values are computed using noiseless statevector simulation. The exact Hamiltonian ground-state energy, obtained through numerical diagonalization, serves as the reference for calculating the energy gap $\Delta E = E - E_0$, where E_0 is the lowest eigenvalue of H and E denotes either the evaluated circuit energy or the directly predicted minimum energy, depending on the approach. The reference energy is not disclosed to the LLM. Unlike the parent-Hamiltonian benchmark, the random-Hamiltonian construction does not guarantee that the chosen ansatz can represent the ground state. Consequently, a nonzero energy gap may reflect both limitations in circuit expressivity and incomplete optimization. Since the minimum energy attainable within the ansatz is not independently established, these contributions cannot be distinguished in the present comparison.

Figure 5(a) compares the absolute energy gaps obtained by Adam, the LMO, and direct LLM energy prediction. Adam progressively reduces the energy gap through iterative optimization, whereas the LMO generally produces parameter configurations with larger gaps and shows limited improvement over subsequent rounds. This suggests that, for general tested Hamiltonians, the symbolic circuit and Hamiltonian descriptions alone provide insufficient information for the LLM to reliably identify low-energy parameter configurations.

Figure 5(b) presents the distribution of signed energy gaps across all configurations. Direct LLM energy prediction



(a) (b)

Figure 5: Comparison of Adam optimization, LMO parameter generation, and direct LLM energy prediction across random Hamiltonian instances with different numbers of qubits and circuit layers. (a) Best absolute energy gap as a function of the number of Hamiltonian expectation-value evaluations. Each trajectory corresponds to an individual Hamiltonian instance. Direct expectation value LLM predictions are displayed at a nominal position of one evaluation for visualization, although they require no quantum circuit evaluations. (b) Distribution of the signed energy gaps across all configurations. Each point represents one Hamiltonian instance, and violins summarize the corresponding distributions. Red crosses indicate direct LLM predictions below the exact ground-state energy, which violate the spectral lower bound.

frequently produces estimates below the true ground-state energy, violating the spectral lower bound. Without prior knowledge of the ground-state energy or an independently established lower bound, such violations cannot generally be identified. Moreover, a directly predicted energy does not provide a quantum state whose expectation value can be independently evaluated. In contrast, the LMO generates explicit circuit parameters that can be used to prepare a quantum state and measure its energy expectation value, even when the true ground-state energy is unknown. By the variational principle, this evaluated energy provides an upper bound on the ground-state energy, subject to statistical and experimental uncertainties. Therefore, although LMO-generated parameters do not necessarily yield lower energy errors, they provide a physically realizable and independently verifiable energy estimate, unlike direct numerical predictions.

B. Circuit interpretability

We evaluate the ability of the frozen LLM to interpret quantum circuits under three equivalent representations: logical, native, and obfuscated. The benchmark comprises Grover's search algorithm [42], the quantum Fourier transform (QFT) [43], and the Bernstein-Vazirani algorithm [44], with five instances per algorithm and representation, yielding 45 independent interpretations. The model receives only the anonymized OpenQASM 3 description of each circuit, without algorithm-specific metadata or access to circuit execution.

Figure 6(a) summarizes algorithm identification accuracy across the three representations. The model correctly identifies all 15 algorithms in the logical representation, compared with 11 of 15 in the native representation and 12 of 15 in the obfuscated representation. Grover's algorithm is identified in 5/5 logical, 4/5 native, and 5/5 obfuscated circuits, while QFT is identified in all 15 cases. The largest reduction occurs for Bernstein-Vazirani, whose identification accuracy decreases from 5/5 in the logical representation to 2/5 in both native and obfuscated representations. These results indicate that algorithm identification is sensitive to the circuit representation, although the effect varies across algorithms.

Algorithm identification does not necessarily reflect whether the model correctly predicts the circuit's computational output. Figure 6(b) reports the accuracy of explicit output bitstring predictions for Grover and Bernstein-Vazirani. Across these 30 interpretations, the model predicts the correct most-likely measurement outcome in 29 cases (96.7%). Grover reaches 5/5 correct predictions in the logical representation, 4/5 in the native representation, and 5/5 in the obfuscated representation. For Bernstein-Vazirani, the predicted output is correct in all 15 cases, including those in which the model does not identify the algorithm by name.

This distinction is particularly evident for Bernstein-Vazirani. Under native decomposition and obfuscation, the model correctly identifies the algorithm in only 2/5 instances per representation, yet predicts the corresponding secret

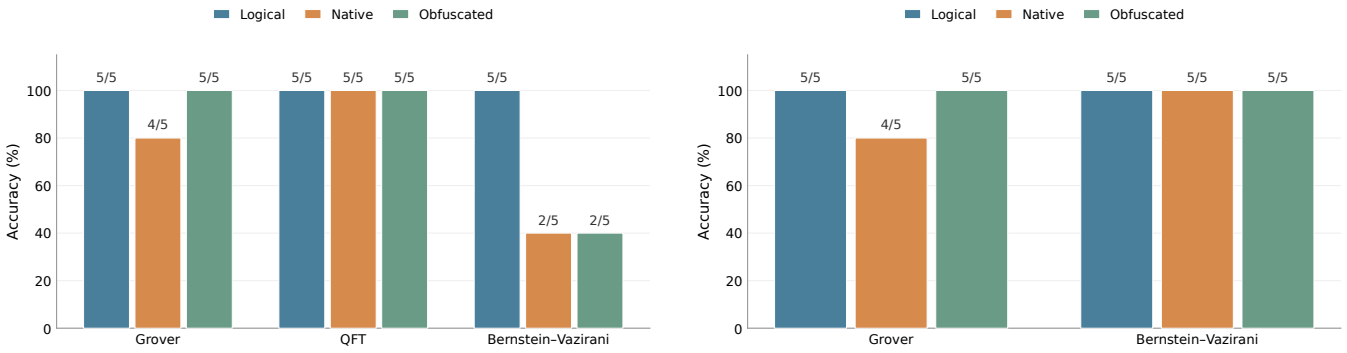


Figure 6: Blind quantum circuit interpretation across logical, native, and obfuscated representations. (a) Accuracy of algorithm identification for Grover, QFT, and Bernstein-Vazirani. (b) Accuracy of the predicted most-likely measurement bitstring for Grover and Bernstein–Vazirani. Each group contains five instances, and labels indicate the number of correct predictions. QFT is excluded from (b) because a single output bitstring does not characterize the Fourier transformation.

bitstring in all five. Thus, a failure to identify the conventional algorithmic family does not necessarily imply a failure to infer the observable computation. The result also suggests that functional predictions can remain accurate when familiar gate patterns are modified by semantics-preserving transformations. For QFT, the model identifies the algorithm in all 15 cases. However, algorithm recognition alone does not establish that the model has correctly characterized the Fourier transformation. In particular, measurement probabilities in the computational basis do not determine the relative phases of the output state. We therefore distinguish successful algorithm identification from the correctness of the model's explanations of phase relationships and interference, which are not systematically evaluated here.

The results show that the LLM can identify familiar quantum algorithms and frequently predict their computational outputs under different circuit representations. The Bernstein-Vazirani results provide a clear example in which functional output prediction remains accurate despite reduced algorithm identification. Nevertheless, the transformed circuits also differ in depth and description length, and the benchmark contains only five instances per algorithm. Consequently, these findings demonstrate representation robustness within the tested circuit families, but do not establish that the model's interpretations are independent of training data patterns or that its explanations faithfully describe its internal reasoning process. Additional implementation details and analysis are provided in Appendix I.

IV. CONCLUSIONS

In this work, we investigated the capabilities and limitations of a frozen, general-purpose large language model for generating parameters of fixed variational quantum circuits from symbolic circuit and Hamiltonian descriptions. The results reveal a clear distinction between general and structured optimization problems. For randomly generated Hamiltonians, the LMO struggles to identify low-energy parameter configurations and does not consistently outperform conventional Adam optimization. In contrast, for structured parent and molecular Hamiltonians, the model can generate promising parameter configurations without prior objective-function feedback, suggesting that identifiable physical and mathematical structure may facilitate parameter inference.

Iterative feedback generally provides limited improvement over the initial parameter proposals, although the physics-aware molecular experiments demonstrate that additional problem-specific information and energy feedback can improve optimization in some cases. We also examined direct LLM predictions of minimum energies, which can violate the Hamiltonian spectral lower bound. Unlike such numerical predictions, LLM-generated circuit parameters define quantum states whose energy expectation values can be independently evaluated, even without knowing the ground-state energy. This distinction highlights the practical importance of physically verifiable parameter proposals.

Beyond parameter optimization, we investigated blind circuit interpretation under different symbolic representations. The model successfully identified several quantum algorithms and frequently predicted their measurement outcomes, including cases where algorithm identification was unsuccessful. These observations suggest that functional output prediction and algorithm recognition are distinct capabilities, although the results do not establish that the model's explanations faithfully reflect its internal reasoning process.

Taken together, these findings suggest that inference-time parameter programming can complement conventional variational optimization when the problem admits exploitable structure. However, the results do not establish a general computational advantage or demonstrate that the model performs general quantum-mechanical reasoning. Its performance may depend on patterns encountered during pretraining, and the structured Hamiltonians considered here may admit specialized classical solution strategies. Furthermore, the cost of language-model inference must be considered alongside quantum objective-evaluation requirements.

DATA AVAILABILITY

The code and data presented in this paper can be found at `https://github.com/tiago939/NeuralOptimizer`.

ACKNOWLEDGEMENTS

This work was supported by the São Paulo Research Foundation (FAPESP), under Grants 2025/27502-3, No. 2023/15739-3, No. 2026/22051-6, No. 2025/15490-0, and No. 2022/00209-6, by the National Council for Scientific and Technological Development (CNPq), grants No. 422316/2023-7, No. 140174/2026-5, and No. 302234/2026-8, and by Petrobrás/CENPES, grant No. 2025/00505-2.

[1] M. Cerezo, A. Arrasmith, R. Babbush, S. C. Benjamin, S. Endo, K. Fujii, J. R. McClean, K. Mitarai, X. Yuan, L. Cincio, and P. J. Coles, Variational quantum algorithms, Nature Reviews Physics **3**, 625 (2021).
[2] A. Peruzzo, J. McClean, P. Shadbolt, M.-H. Yung, X.-Q. Zhou, P. J. Love, A. Aspuru-Guzik, and J. L. O'Brien, A variational eigenvalue solver on a photonic quantum processor, Nature Communications **5**, 4213 (2014).
[3] M. Schuld, V. Bergholm, C. Gogolin, J. Izaac, and N. Killoran, Evaluating analytic gradients on quantum hardware, Phys. Rev. A **99**, 032331 (2019).
[4] J. R. McClean, S. Boixo, V. N. Smelyanskiy, R. Babbush, and H. Neven, Barren plateaus in quantum neural network training landscapes, Nature Communications **9**, 4812 (2018).
[5] M. Andrychowicz, M. Denil, S. Gomez, M. W. Hoffman, D. Pfau, T. Schaul, B. Shillingford, and N. de Freitas, Learning to learn by gradient descent by gradient descent (2016), arXiv:1606.04474.
[6] O. Wichrowska, N. Maheswaranathan, M. W. Hoffman, S. G. Colmenarejo, M. Denil, N. de Freitas, and J. Sohl-Dickstein, Learned optimizers that scale and generalize (2017).
[7] L. Metz, C. D. Freeman, J. Harrison, N. Maheswaranathan, and J. Sohl-dickstein, Practical tradeoffs between memory, compute, and performance in learned optimizers, in *Proceedings of The 1st Conference on Lifelong Learning Agents*, Proceedings of Machine Learning Research, Vol. 199, edited by S. Chandar, R. Pascanu, and D. Precup (PMLR, 2022) pp. 142–164.
[8] A. Moudgil, B. Knyazev, G. Lajoie, and E. Belilovsky, Celo: Training versatile learned optimizers on a compute diet, Transactions on Machine Learning Research (2025).
[9] X. Bai, J.-H. Liang, J. Teoh, and V. Sitzmann, Reactive Optimizers (2026).
[10] G. Verdon, M. Broughton, J. R. McClean, K. J. Sung, R. Babbush, Z. Jiang, H. Neven, and M. Mohseni, Learning to learn with quantum neural networks via classical neural networks (2019), arXiv:1907.05415.
[11] S. Khairy, R. Shaydulin, L. Cincio, Y. Alexeev, and P. Balaprakash, Learning to optimize variational quantum circuits to solve combinatorial problems, in *Proceedings of the AAAI Conference on Artificial Intelligence*, Vol. 34 (2020) pp. 2367–2375.
[12] L. Friedrich and J. Maziero, Learning to learn with an evolutionary strategy applied to variational quantum algorithms, Physical Review A **111**, 022630 (2025).
[13] H. Zou, M. Rahm, A. F. Kockum, and S. Olsson, Generative flow-based warm start of the variational quantum eigensolver, npj Quantum Information **12**, 5 (2025).
[14] M. Wilson, R. Stromswold, F. Wudarski, S. Hadfield, N. M. Tubman, and E. G. Rieffel, Optimizing quantum heuristics with meta-learning, Quantum Machine Intelligence **3**, 13 (2021).
[15] K. Chen, H. Matsuyama, and W. Huang, Learning to learn with quantum optimization via quantum neural networks, in *2025 IEEE International Conference on Quantum Computing and Engineering (QCE)*, Vol. 01 (2025) pp. 01–12.
[16] J. Falla, Q. Langfitt, Y. Alexeev, and I. Safro, Graph representation learning for parameter transferability in quantum approximate optimization algorithm, Quantum Machine Intelligence **6**, 46 (2024).
[17] I. Lyngfelt and L. García-Álvarez, Symmetry-informed transferability of optimal parameters in the quantum approximate optimization algorithm, Phys. Rev. A **111**, 022418 (2025).
[18] Y. Wang, B. Qi, C. Ferrie, and D. Dong, Trainability enhancement of parameterized quantum circuits via reduced-domain parameter initialization, Phys. Rev. Appl. **22**, 054005 (2024).

[19] C. Yang, X. Wang, Y. Lu, H. Liu, Q. V. Le, D. Zhou, and X. Chen, Large Language Models as Optimizers (2024).

[20] B. Huang, X. Wu, Y. Zhou, J. Wu, L. Feng, R. Cheng, and K. C. Tan, Exploring the True Potential: Evaluating the Black-box Optimization Capability of Large Language Models (2024).

[21] S. Huang, K. Yang, S. Qi, and R. Wang, When large language model meets optimization, Swarm and Evolutionary Computation **90**, 101663 (2024).

[22] J. Meindl, Y. Tian, T. Cui, V. Thost, Z.-W. Hong, J. Chen, W. Matusik, and M. K. Luković, SemanticOpt: Towards LLM-Based Semantic Black-Box Optimization (2026).

[23] J. Wang, Y. Zhang, and X. Li, NeuroGen: Neural Network Parameter Generation via Large Language Models (2025).

[24] R. Takehi, J. Teoh, A. Zhang, and O. Khattab, Sparks of Weight-Space Programming: LLMs can natively read & write neural network weights, `https://rikiyat.github.io/blog/weight-space-programming/` (2026), blog post.

[25] D. Kundu, S. Ghosh, and V. G. Honavar, Weight-space programming of variational quantum circuits: Large language models write quantum circuit parameters without an optimizer (2026), arXiv:2611.11537.

[26] L. Jern, V. Uotila, C. Yu, and B. Zhao, Agent-q: Fine-tuning large language models for quantum circuit generation and optimization, in *2025 IEEE International Conference on Quantum Computing and Engineering (QCE)* (IEEE, 2025) p. 1621–1632.

[27] J. Zhuang and C. Guan, Large language models can help mitigate barren plateaus in quantum neural networks, in *Findings of the Association for Computational Linguistics: ACL 2026*, edited by M. Liakata, V. P. Moreira, J. Zhang, and D. Jurgens (Association for Computational Linguistics, San Diego, California, United States, 2026) pp. 10751–10767.

[28] A. Macarone-Palmieri and R. L. Franco, Quantum circuit generation via test-time learning with large language models (2026), arXiv:2602.03466.

[29] I. Tyagin, M. H. Farag, K. Sherbert, K. Shirali, Y. Alexeev, and I. Safro, QAOA-GPT: Efficient Generation of Adaptive and Regular Quantum Approximate Optimization Algorithm Circuits (2025).

[30] K. Sakka, W. Mizukami, and K. Mitarai, An LLM System for Autonomous Variational Quantum Circuit Design (2026).

[31] N. N. Nguyen, T. T. Vu, J. Le, H. K. Dam, D. H. Duong, and D. T. Hoang, BRIDG-Q: Barren-Plateau-Resilient Initialisation with Data-Aware LLM-Generated Quantum Circuits (2026).

[32] A. Cross, A. Javadi-Abhari, T. Alexander, N. De Beaudrap, L. S. Bishop, S. Heidel, C. A. Ryan, P. Sivarajah, J. Smolin, J. M. Gambetta, and B. R. Johnson, Openqasm3: A broader and deeper quantum assembly language, ACM Transactions on Quantum Computing **3**, 10.1145/3505636 (2022).

[33] K. Kabra, C. Venhoff, and C. S. d. Witt, Weight Oracles: Reading Neural Network Weights with Language Models (2026).

[34] M. Chen, J. Cheng, P. Li, H. Wang, T. Chen, and J. Liu, Symbolic analysis of Grover search algorithm via Chain-of-Thought reasoning and quantum-native tokenization, npj Quantum Information **12**, 48 (2026).

[35] N. K. Mondal, Quantumsemeval: Benchmarking LLMs' understanding of quantum programs via semantic equivalence checking, in *Deep Learning for Code: Towards Human-Centered Coding Agents* (2026).

[36] H. Wang, P. Li, M. Chen, J. Cheng, J. Liu, and T. Chen, GroverGPT: A Large Language Model with 8 Billion Parameters for Quantum Searching (2025).

[37] M. Afane, K. Laufer, W. Wei, Y. Mao, J. Farooq, Y. Wang, and J. Chen, Quantum-Audit: Evaluating the Reasoning Limits of LLMs on Quantum Computing (2026).

[38] E. Seefried, R. Ghosh, S. Afrose, N. Stapleton, V. L. Ortega, T. Humble, and T. Ghosal, Benchmarking the Quantum Leap: Auditing LLM Evaluation for Quantum Code Generation (2026).

[39] Y. Alexeev, M. H. Farag, T. L. Patti, M. E. Wolf, N. Ares, A. Aspuru-Guzik, S. C. Benjamin, Z. Cai, S. Cao, C. Chamberland, Z. Chandani, F. Fedele, I. Hamamura, N. Harrigan, J.-S. Kim, E. Kyoseva, J. G. Lietz, T. Lubowe, A. McCaskey, R. G. Melko, K. Nakaji, A. Peruzzo, P. Rao, B. Schmitt, S. Stanwyck, N. M. Tubman, H. Wang, and T. Costa, Artificial intelligence for quantum computing, Nature Communications **16**, 10829 (2025).

[40] D. P. Kingma and J. Ba, Adam: A method for stochastic optimization, in *International Conference on Learning Representations (ICLR)* (2015).

[41] J. Romero, R. Babbush, J. R. McClean, C. Hempel, P. J. Love, and A. Aspuru-Guzik, Strategies for quantum computing molecular energies using the unitary coupled cluster ansatz, Quantum Science and Technology **4**, 014008 (2018).

[42] L. K. Grover, A fast quantum mechanical algorithm for database search, in *Proceedings of the Twenty-Eighth Annual ACM Symposium on Theory of Computing*, STOC '96 (Association for Computing Machinery, New York, NY, USA, 1996) p. 212–219.

[43] P. Shor, Algorithms for quantum computation: discrete logarithms and factoring, in *Proceedings 35th Annual Symposium on Foundations of Computer Science* (1994) pp. 124–134.

[44] E. Bernstein and U. Vazirani, Quantum complexity theory, SIAM Journal on Computing **26**, 1411 (1997).

[45] W. J. Hehre, R. F. Stewart, and J. A. Pople, Self-consistent molecular-orbital methods. i. use of gaussian expansions of slater-type atomic orbitals, Journal of Chemical Physics **51**, 2657 (1969).

[46] M. Born and R. Oppenheimer, Zur quantentheorie der molekeln, Annalen der Physik **389**, 457 (1927), https://onlinelibrary.wiley.com/doi/pdf/10.1002/andp.19273892002.

[47] P. Jordan and E. Wigner, Über das Paulische Äquivalenzverbot, Zeitschrift für Physik **47**, 631 (1928).

[48] F. Kobayashi, K. Mitarai, and K. Fujii, Parent hamiltonian as a benchmark problem for variational quantum eigensolvers, Phys. Rev. A **105**, 052415 (2022).

Appendix A: System Prompts

This appendix documents the instructions and input formats used for circuit optimization and blind circuit interpretation. The system instructions remain fixed within each experimental protocol, while the user prompts contain instance-specific information.

1. Blind optimization prompt

For circuit optimization, the language model receives a fixed parameterized circuit expressed in OpenQASM 3 and a Hamiltonian represented by its Pauli decomposition. The system instructions require the model to propose a complete numerical parameter vector that minimizes the Hamiltonian expectation value, without modifying the circuit or Hamiltonian. The parameter ordering and Pauli labeling conventions are explicitly specified.

Blind optimization - System prompt

```
You optimize the expectation value of a supplied Hamiltonian using a fixed parameterized quantum circuit. Choose
    one complete absolute numerical parameter vector in radians. Do not modify the circuit or Hamiltonian. Infer
    parameter order from the OpenQASM 3 input declarations in their textual order. Qiskit Pauli labels run from q[
    n-1] on the left to q[0] on the right. Use only the provided circuit, Hamiltonian, optional noise model,
    optional measurement specification, and previous angle-energy observations. Return only a JSON object with
    keys "theta" (numeric array) and "mechanism" (brief, testable reasoning).
```

The user prompt contains the circuit description and Hamiltonian coefficients. Depending on the experimental configuration, additional fields provide information about the noise model, measurement budget, and previous parameter evaluations. Its structure is illustrated below.

Blind optimization - User prompt structure

```
CIRCUIT_OPENQASM_3:
<parameterized OpenQASM 3 circuit>

HAMILTONIAN_PAULI_TERMS:
[
  {
    "pauli": "<Pauli string>",
    "coefficient": <numerical value>
  },
  ...
]

NOISE_MODEL:
<optional JSON noise specification>

MEASUREMENT_SPECIFICATION:
{
  "shots_per_energy_evaluation": <integer>
}

PREVIOUS_EVALUATIONS:
[
  {
    "theta": [<numerical parameters>],
    "energy": <numerical energy>
  },
  ...
]
```

The first proposal is generated without previous objective-function evaluations. In subsequent rounds, the prompt may include the parameter vectors and corresponding energy estimates obtained from earlier evaluations. Noise information and measurement specifications are disclosed only when applicable. The model returns a JSON object containing the complete parameter vector and a brief explanation of its proposed solution. This explanation is recorded

but does not influence the numerical evaluation of the candidate.

2. Physics-aware prompt

For molecular problems, the LMO receives the same circuit and Hamiltonian information as in the standard configuration, supplemented with chemical context derived from the molecular system. This additional information includes the molecular geometry, basis set, electronic configuration, active space, qubit mapping, and reference state. The circuit and Hamiltonian remain fixed, and the model is instructed to return a complete parameter vector without modifying either representation.

Physics-aware optimization - System prompt

```
You optimize the expectation value of a supplied Hamiltonian
using a fixed parameterized quantum circuit.
Choose one complete absolute numerical parameter vector in radians.
Do not modify the circuit or Hamiltonian.
Infer parameter order from the OpenQASM 3 input declarations
in their textual order.
Qiskit Pauli labels run from q[n-1] on the left to q[0] on the right.
Use only the provided circuit, Hamiltonian, chemical context
(when present), optional noise model, and previous
angle-energy observations.
Return only a JSON object with keys "theta" (numeric array)
and "mechanism" (brief, testable reasoning).
```

The user prompt follows the standard structure, with an additional chemical-context section:

Physics-aware optimization - User prompt

```
CIRCUIT_OPENQASM_3:
<parameterized OpenQASM 3 circuit>

HAMILTONIAN_PAULI_TERMS:
<Pauli strings and coefficients>

NOISE_MODEL:
<noise information, when disclosed>

PREVIOUS_EVALUATIONS:
<previous parameter vectors and evaluations, when available>

CHEMICAL_CONTEXT:
{
  "molecule": "<molecule name>",
  "geometry_angstrom": "<atomic coordinates>",
  "basis": "<basis set>",
  "charge": "<molecular charge>",
  "multiplicity": "<spin multiplicity>",
  "full_spatial_orbitals": "<number>",
  "full_num_particles": "<spin-resolved electron counts>",
  "active_spatial_orbitals": "<number>",
  "active_num_particles": "<spin-resolved active electron counts>",
  "active_orbital_indices": "<selected orbital indices>",
  "n_qubits": "<number>",
  "ansatz": "<ansatz name>",
  "mapping": "Jordan-Wigner",
  "reference_state": "Hartree-Fock; preparation included in the OpenQASM",
  "hf_basis_index": "<Hartree-Fock basis index>",
  "initial_theta": "<initial parameters, when available>",
  "shots_per_energy_query": "<number of shots>",
  "noise": "<true or false>",
  "energy_convention": "Hamiltonian Pauli coefficients describe electronic
  energy. Observed feedback uses electronic energy, excluding additive
```

```
  nuclear and frozen-core offsets."
}
```

The chemical context is constructed from the molecular problem definition rather than inferred by the language model. Reference ground-state energies are not included in the prompt. The noise-model and previous-evaluation sections are included only when applicable. Apart from the additional chemical context, the standard prompt structure and parameter-output format remain unchanged.

3. Circuit interpretability prompt

For blind circuit interpretation, the language model receives an anonymized OpenQASM 3 description. The instructions require the model to distinguish mathematical conclusions from hypotheses about the circuit's computational purpose and to report uncertainty when appropriate.

Circuit interpretation - System prompt

```
You are analyzing an unknown quantum circuit from its OpenQASM 3 description.
Use ONLY the supplied circuit. Do not use external tools, simulators, or experiments.
Do not assume a particular named algorithm. Distinguish verifiable mathematical
conclusions from hypotheses about the circuit's intended computational task.
If the algorithm's purpose is ambiguous, report the ambiguity explicitly.
Qubit indices start at q[0]; classical bit strings are written in descending
bit order, with the highest-index classical bit on the left.

Return ONLY one valid JSON object with these keys:
{
  "circuit_behavior": "Mathematical behavior of the circuit, with supporting details.",
  "algorithm_hypothesis": "Best-fitting algorithm name or 'not identifiable'.",
  "predicted_measurement_behavior": "Plain-language prediction of measurement outcomes.",
  "predicted_most_likely_bitstring": "One most likely bitstring in descending classical-bit order, or null if
     uncertain.",
  "evidence": ["Concrete gate-level evidence."],
  "alternative_hypotheses": ["Other possible interpretations."],
  "not_identifiable": ["Properties not identifiable from the circuit alone."],
  "confidence": 0.0
}
The example predicted_probabilities entry is illustrative, not an actual prediction.
For measured circuits, provide a normalized bitstring-to-probability object when
possible, covering all outcomes with non-negligible probability. You may provide
an empty object if you cannot infer quantitative probabilities. Never invent
an algorithm label or probabilities when uncertain. Confidence refers to the
algorithm identification, not mathematical correctness.
```

The user prompt contains only the anonymized circuit:

Circuit interpretation – User prompt

```
OPENQASM_3:
<anonymized OpenQASM 3 circuit>
```

The same instructions are used for logical, native, and obfuscated representations. Algorithm-specific identifiers and comments are removed before inference. The model's predictions are subsequently compared with independently established circuit properties.

Appendix B: Molecular Hamiltonians and Circuit Construction

This appendix describes the construction of the molecular Hamiltonians, their representation as qubit operators, and the parameterized circuits used in the molecular optimization experiments.

We consider neutral singlet H_4 and LiH, both described using the STO-3G basis [45]. For H_4, we retain the full STO-3G orbital space, containing four electrons and four spatial orbitals. For LiH, we employ a reduced active space containing two electrons and three spatial orbitals. Their atomic coordinates are given in Appendices C and D, respectively. The same Hamiltonian and circuit architecture are used for the LMO and classical optimization baselines within each molecular benchmark.

Within the Born-Oppenheimer approximation [46], the electronic Hamiltonian of a molecular system is expressed in second quantization as

$$H_{\mathrm{el}} = \sum_{pq} h_{pq} a_p^\dagger a_q + \frac{1}{2} \sum_{pqrs} h_{pqrs} a_p^\dagger a_q^\dagger a_s a_r, \tag{B1}$$

where $a_p^\dagger$ and a_p are fermionic creation and annihilation operators, respectively. The coefficients h_{pq} and h_{pqrs} are the one- and two-electron integrals in the chosen orbital basis. The molecular energy additionally includes nuclear repulsion and, when an active-space approximation is employed, the energy associated with inactive electrons.

The electronic Hamiltonian is mapped to qubit operators using the Jordan-Wigner transformation [47]. The resulting qubit Hamiltonian takes the form

$$H_{\mathrm{qubit}} = \sum_{j=1}^{M} c_j P_j, \tag{B2}$$

where c_j are real coefficients and P_j are tensor products of Pauli operators. The physical molecular energy is calculated as

$$E_{\mathrm{mol}}(\boldsymbol{\theta}) = \langle \psi(\boldsymbol{\theta}) | H_{\mathrm{qubit}} | \psi(\boldsymbol{\theta}) \rangle + E_{\mathrm{offset}}, \tag{B3}$$

where E_{offset} accounts for constant energy contributions excluded from the mapped qubit Hamiltonian.

The variational state is prepared using a fixed parameterized quantum circuit,

$$|\psi(\boldsymbol{\theta})\rangle = U(\boldsymbol{\theta}) |\psi_{\mathrm{ref}}\rangle, \tag{B4}$$

where $|\psi_{\mathrm{ref}}\rangle$ denotes the Hartree–Fock reference state and $\boldsymbol{\theta}$ contains the variational parameters. For the LiH benchmark, we employ a unitary coupled-cluster ansatz with single and double excitations (UCCSD) [41]. The circuit architecture remains unchanged during optimization, with both the LMO and classical optimizers modifying only the numerical parameter values.

For LMO inference, the parameterized circuit is serialized into OpenQASM 3, and the Hamiltonian is provided as a list of Pauli strings and their coefficients. The parameter ordering is explicitly defined to ensure consistency between the generated values and the circuit. Optimization performance is evaluated using the energy error relative to the corresponding full configuration interaction (FCI) reference,

$$\Delta E(\boldsymbol{\theta}) = E_{\mathrm{mol}}(\boldsymbol{\theta}) - E_{\mathrm{FCI}}. \tag{B5}$$

The reference energy is obtained by diagonalizing the molecular Hamiltonian within the relevant physical electron-number and spin sector. We adopt the conventional chemical-accuracy threshold of 1 kcal/mol, corresponding approximately to $\epsilon_{\mathrm{chem}} \simeq 1.59 \times 10^{-3}\, E_h$.

Appendix C: LiH Molecule

We further evaluate the LMO on the molecular ground-state energy problem of lithium hydride (LiH) molecule, which is defined by the following Cartesian coordinates in angstroms:

$$\mathrm{Li}: \ (0, 0, 0), \qquad \mathrm{H}: \ (0, 0, 1.60). \tag{C1}$$

The electronic Hamiltonian is constructed using the STO-3G basis [45] and an active-space approximation containing two electrons. The fermionic Hamiltonian is mapped to qubit operators using the Jordan-Wigner transformation [47].

The variational state is prepared using a unitary coupled-cluster ansatz with single and double excitations (UCCSD) [41], initialized from the Hartree-Fock reference state. The circuit architecture remains fixed throughout optimization with only its numerical parameters being updated.

As in the H_4 experiment, we investigate the standard blind and physics-aware prompting configurations for the lithium hydride (LiH) molecule. Both use the same frozen LLM to generate complete parameter vectors, which are evaluated using the molecular Hamiltonian. The physics-aware configuration is evaluated in three repeated runs, while one standard blind-prompt run is included for comparison. The resulting trajectories are compared with Adam using the cumulative number of Hamiltonian energy evaluations. Figure 7 presents the energy errors relative to the active-space full configuration interaction (FCI) reference. All four LMO runs achieve energy errors near numerical precision within the first few evaluations. In contrast, Adam begins with a substantially larger energy error and requires considerably more objective evaluations to reach the chemical-accuracy threshold.

The LMO trajectories remain close to the reference energy across subsequent proposals, with only small differences between repeated runs. These results demonstrate that the LMO can generate near-ground-state parameter configurations for the tested LiH problem with a small number of objective evaluations. However, the comparison concerns quantum objective-evaluation requirements rather than total computational cost, and the limited number of runs does not establish a systematic advantage of physics-aware prompting over the blind configuration.

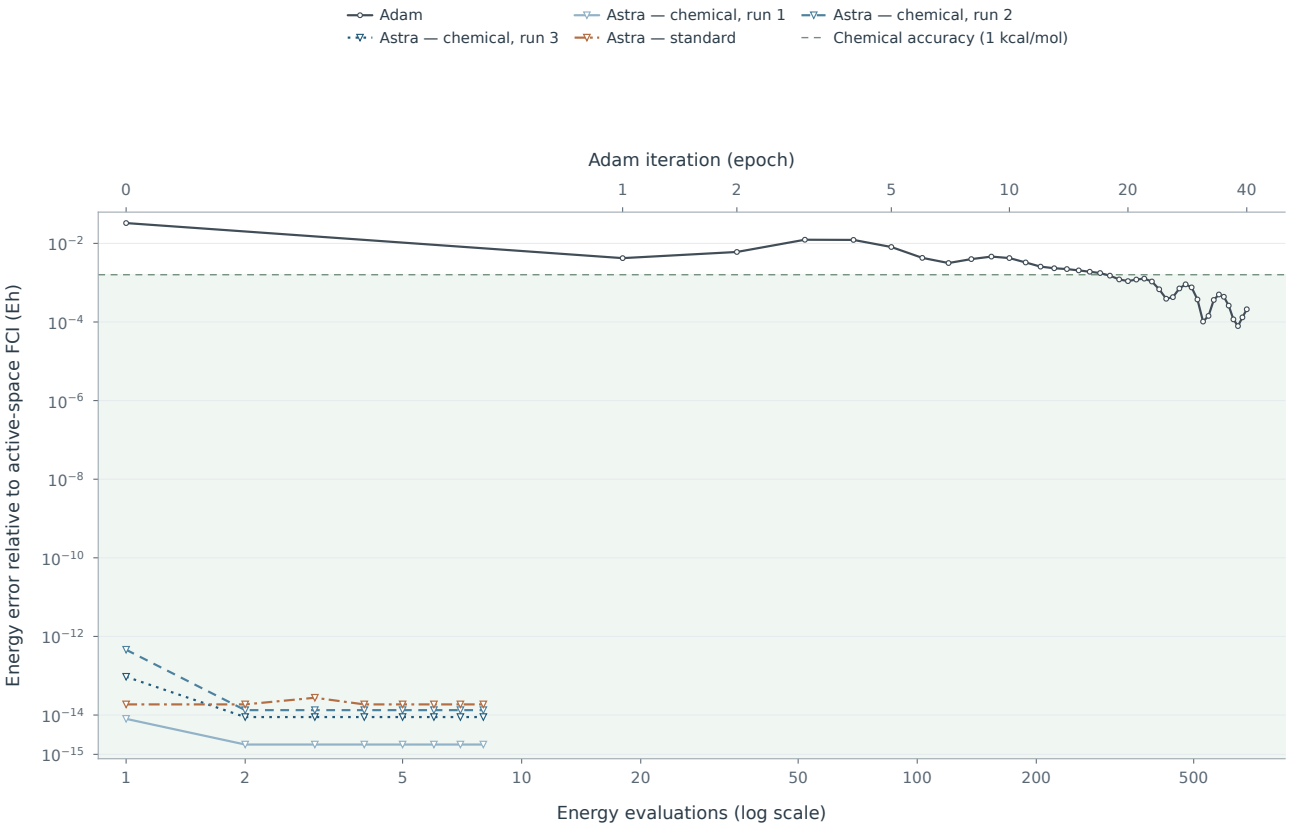


Figure 7: Optimization of the LiH molecular Hamiltonian using Adam and the language model optimizer. Three runs with the physics-aware (chemical) prompt and one run with the standard blind prompt are shown. The vertical axis represents the energy error relative to the active-space full configuration interaction reference, while the horizontal axis shows the cumulative number of Hamiltonian energy evaluations on a logarithmic scale. The dashed horizontal line indicates the chemical-accuracy threshold of 1 kcal/mol. The upper horizontal axis indicates the corresponding Adam optimization iterations.

Appendix D: H_4 Molecule

We examine two geometries of neutral singlet H_4 using STO-3G. The standard reference structure is a planar rectangle, while the second is a nonplanar and in-plane distorted structure. Both configurations contain four electrons

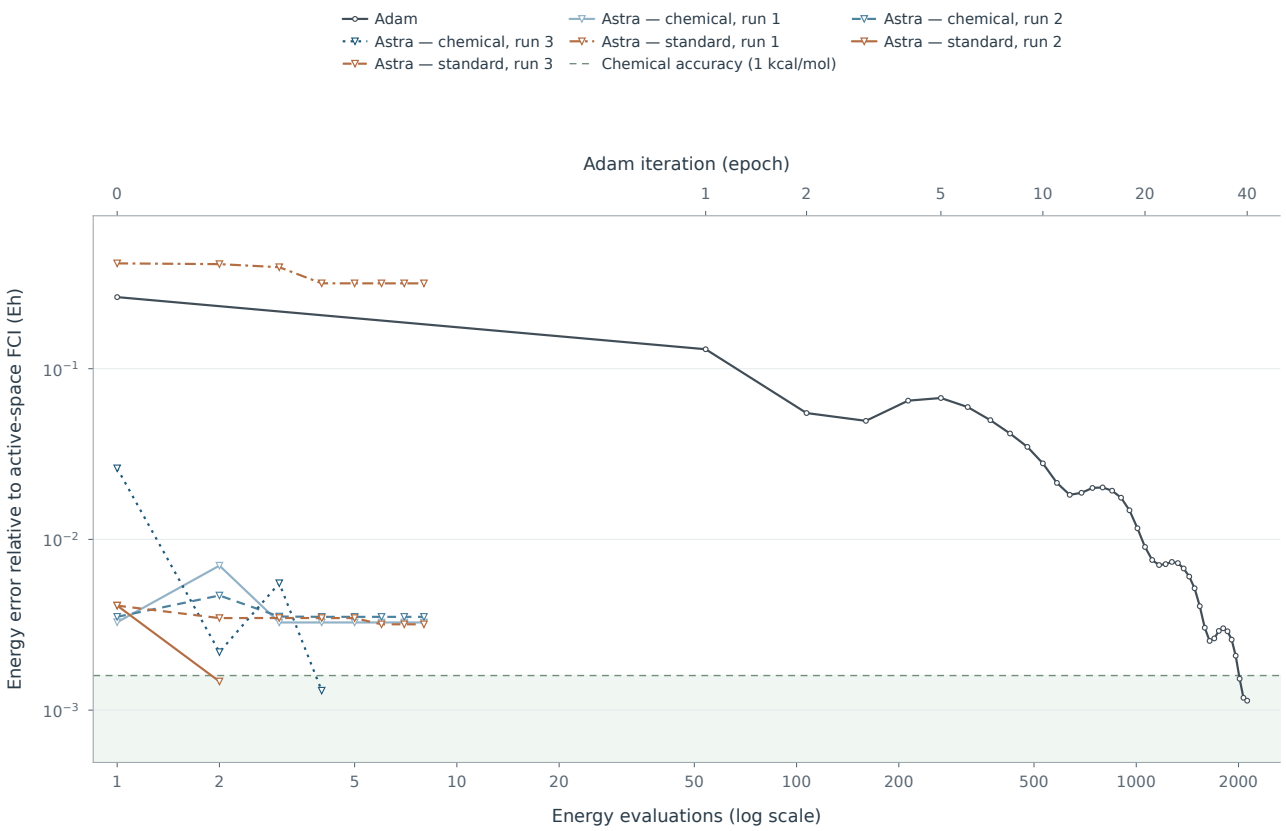


Figure 8: Optimization trajectories for the distorted H_4 Hamiltonian corresponding to the nonplanar coordinates in Table I. The fixed eight-qubit, 26-parameter UCCSD circuit is optimized with the standard (blind) and physics-aware (chemical) LMO prompts, with three independent runs per prompt, and compared with Adam. The vertical axis shows the energy error from the FCI reference of the distorted Hamiltonian; the lower horizontal axis gives cumulative Hamiltonian energy evaluations on a logarithmic scale. The upper axis shows Adam iterations. The dashed line and shaded region mark chemical accuracy $1\,\mathrm{kcal\,mol^{-1}}$.

in four spatial orbitals, without frozen-core or active-space truncation. Their coordinates are given in Table I.

Table I: Cartesian geometries of the standard and distorted H_4 molecules, in angstroms.

	Standard H_4			Distorted H_4		
Atom	x	y	z	x	y	z
H_1	0.00	0.00	0.00	0.00	0.00	0.00
H_2	1.06	0.00	0.00	1.00	0.00	0.00
H_3	0.00	1.20	0.00	0.00	1.20	0.20
H_4	1.06	1.20	0.00	1.05	1.20	−0.20

The standard geometry is the one in the main text, Fig. 4. The distorted geometry was introduced as an additional generalization probe. In particular, the blind-prompt test assesses whether parameter proposals that may exploit familiar molecular patterns remain effective if Hamiltonian differs from that of the standard configuration. This comparison is intended to test sensitivity to the molecular instance. Because the chemical-context prompt discloses the molecular geometry and electronic setting, the blind configuration is especially relevant when examining the response to the modified Hamiltonian without that information.

The results for the planar geometry appear in Fig. 4 and the distorted-geometry trajectories appear in Fig. 8. In the distorted case, the quality of LMO-generated parameters varies substantially across independent runs. Some runs approach or cross the chemical-accuracy threshold, while one blind-prompt trajectory remains well above it. These results illustrate the sensitivity of the LMO's performance to the molecular Hamiltonian, although they do not, by

themselves, establish whether the model relies on previously seen data.

Appendix E: Random Parent Hamiltonian

We construct a family of variational optimization problems using parent Hamiltonians, following the benchmark construction principle of Kobayashi et al. [48]. This approach provides Hamiltonians with known ground-state energies whose ground states are guaranteed to be representable by the chosen parameterized circuits. The ansatz $U(\boldsymbol{\theta})$ consists of alternating blocks of single-qubit $R_Y R_Z R_Y$ rotations and fixed nearest-neighbor $R_{XX}(\pi/2)$ entangling gates. For each instance, a hidden parameter vector $\boldsymbol{\theta}^*$ is sampled and used to construct

$$H = U(\boldsymbol{\theta}^*) H_0 U^\dagger(\boldsymbol{\theta}^*), \qquad H_0 = \sum_{q=0}^{n-1} \frac{I - Z_q}{2}. \tag{E1}$$

Since unitary conjugation preserves the spectrum, H has a unique ground state $U(\boldsymbol{\theta}^*)\,|0\rangle^{\otimes n}$, ground-state energy $E_0 = 0$, and spectral gap equal to one. To control the size of the Pauli decomposition, the hidden parameters are sampled predominantly from the Clifford angles $\{0, \pm\pi/2, \pi\}$, while r selected rotations receive non-Clifford angles. This limits the proliferation of Pauli terms while retaining a continuously parameterized optimization circuit. Instances are accepted subject to limits on the number of nonzero Pauli terms and compiled circuit depth. The LMO receives the parameterized circuit and the resulting Pauli Hamiltonian, but neither the hidden parameters nor the construction procedure. Its objective is to find any parameter vector that prepares a low-energy state, rather than to recover the original hidden angles. Further construction details are provided in Appendix F.

We evaluate the LMO on circuits with $n \in \{4, 8, 12\}$ qubits, $L \in \{1, 2, 4\}$ entangling layers, and $r \in \{1, 2\}$ non-Clifford rotations in the generating circuit. Five independently generated instances are considered for each configuration, yielding 90 optimization problems. For each instance, the frozen LMO proposes a complete parameter vector without receiving any objective-function evaluations. Subsequent proposals use feedback from previous energy evaluations, with up to five proposals per instance. All energies in this experiment are evaluated using exact, noiseless statevector simulations. We define a successful solution by an energy gap $E(\boldsymbol{\theta}) - E_0 \leq 10^{-6}$.

Figure 9(a) shows the distribution of first-proposal energy gaps across the 90 instances. Without prior objective feedback, the LMO reaches the target accuracy in 40 of 45 instances (88.9%) for $r = 1$ and 37 of 45 instances (82.2%) for $r = 2$. Most successful proposals achieve energy gaps near numerical precision, whereas the unsuccessful instances exhibit substantially larger errors. These results demonstrate that the LMO can generate near-ground-state parameters directly from symbolic circuit and Hamiltonian descriptions for a substantial fraction of the tested problems.

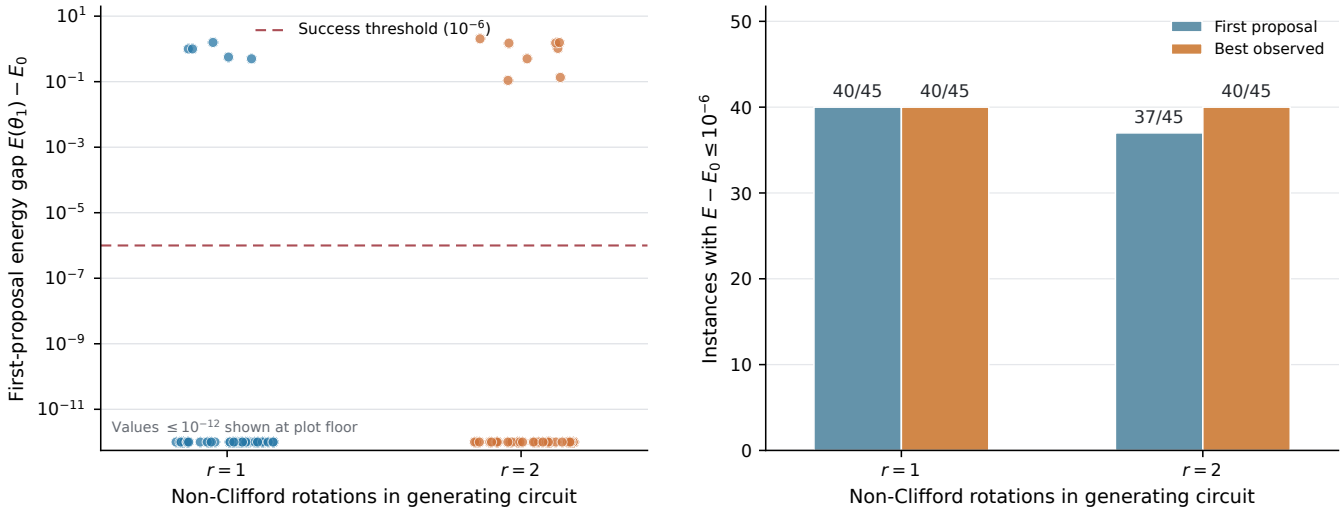
Allowing the LMO to incorporate energy feedback increases the number of successful instances for $r = 2$ from 37 to 40, as shown in Fig. 9(b). For $r = 1$, the number of successful instances remains at 40, although feedback reduces the energy in some initially unsuccessful cases. Across both families, the best observed proposals reach the target accuracy in 80 of 90 instances (88.9%). These observations indicate that feedback can refine initially unsuccessful proposals, although its effect varies across instances.

A comparison with the gradient-based Adam optimizer further highlights the difference in objective-evaluation requirements. While Adam generally requires repeated parameter-shift gradient evaluations to approach low-energy solutions, the LMO frequently identifies near-ground-state parameters in its first proposal, without prior objective feedback. This comparison concerns the number of Hamiltonian evaluations rather than total computational cost, as the LMO additionally performs language-model inference and has access to the symbolic problem description. Detailed optimization trajectories and resource accounting are presented in Appendix G.

Further structural analysis shows that successful state preparation does not generally require recovery of the hidden generating parameters. The LMO often achieves near-unit ground-state fidelity despite substantial differences between the proposed and planted parameter vectors. Moreover, rounding the proposed angles to Clifford-compatible values causes all 90 first proposals to exceed the success threshold, indicating the importance of continuous rotation values. The model-generated explanations also contain physically testable claims, although their consistency with numerical calculations is not guaranteed. These findings are specific to the structured parent-Hamiltonian family and do not establish a general computational advantage. Additional analyses are provided in Appendix H.

Appendix F: Parent Hamiltonian Construction

This appendix describes the parameterized circuit, the generation of random parent Hamiltonians, and the constraints used to obtain instances with a controlled number of Pauli terms. The construction guarantees an exactly



(a) (b)

Figure 9: Performance of the language model optimizer on random parent Hamiltonians with $r = 1$ and $r = 2$ non-Clifford rotations in the generating circuit. (a) Distribution of first-proposal energy gaps for 45 instances per family, obtained without prior objective-function feedback. The dashed line indicates the success threshold of 10^{-6}; gaps below 10^{-12} are displayed at the numerical plotting floor. (b) Number of instances reaching the success threshold on the first proposal and at any observed optimization round. All energies are evaluated using exact, noiseless simulations.

representable ground state while allowing the complexity of the generated Hamiltonian to vary independently of the number of trainable circuit parameters.

1. Parameterized Circuit

We consider an n-qubit circuit $U(\boldsymbol{\theta})$ acting on the initial state $|0\rangle^{\otimes n}$, where $\boldsymbol{\theta} \in \mathbb{R}^p$ contains the trainable rotation angles. The resulting state is

$$|\psi(\boldsymbol{\theta})\rangle = U(\boldsymbol{\theta})\,|0\rangle^{\otimes n}\,. \tag{F1}$$

The ansatz alternates complete single-qubit rotation blocks with fixed entangling layers. Each rotation block applies $R_Y R_Z R_Y$ to every qubit. In chronological gate order, the corresponding unitary is

$$B_\ell(\boldsymbol{\theta}_\ell) = \bigotimes_{q=0}^{n-1} R_Y(\gamma_{\ell,q}) R_Z(\beta_{\ell,q}) R_Y(\alpha_{\ell,q}), \tag{F2}$$

where $\alpha_{\ell,q}$, $\beta_{\ell,q}$, and $\gamma_{\ell,q}$ are independent parameters. The rightmost operator acts first.

The entangling layers contain fixed nearest-neighbor gates,

$$E_\ell = \prod_{\substack{q=\ell \bmod 2 \\ q<n-1}}^{\text{step } 2} R_{XX}^{(q,q+1)}\left(\frac{\pi}{2}\right), \tag{F3}$$

where

$$R_{XX}(\phi) = \exp\left(-i\frac{\phi}{2} X \otimes X\right). \tag{F4}$$

The interacting pairs alternate between even- and odd-indexed connections. For L entangling layers, the complete circuit is

$$U(\boldsymbol{\theta}) = B_L E_{L-1} B_{L-1} \cdots E_1 B_1 E_0 B_0. \tag{F5}$$

There are $L+1$ rotation blocks, giving $p = 3n(L+1)$ trainable parameters. All rotation angles remain independently adjustable during optimization.

2. Reference and Parent Hamiltonians

The reference Hamiltonian is defined as

$$H_0 = \sum_{q=0}^{n-1} \frac{I - Z_q}{2}, \tag{F6}$$

where Z_q acts on qubit q. Its eigenstates are the computational-basis states, with eigenvalues equal to their Hamming weights:

$$H_0 |x\rangle = w_H(x) |x\rangle , \qquad x \in \{0,1\}^n. \tag{F7}$$

Consequently, H_0 has the unique ground state $|0\rangle^{\otimes n}$, ground-state energy zero, and spectral gap one. For each benchmark instance, a hidden parameter vector $\boldsymbol{\theta}^*$ is selected and inserted into the ansatz. The resulting unitary $U^* = U(\boldsymbol{\theta}^*)$ defines the parent Hamiltonian

$$H = U^* H_0 U^{*\dagger}. \tag{F8}$$

By construction,

$$\begin{aligned} HU^* |0\rangle^{\otimes n} &= U^* H_0 U^{*\dagger} U^* |0\rangle^{\otimes n} \\ &= U^* H_0 |0\rangle^{\otimes n} \\ &= 0. \end{aligned} \tag{F9}$$

Therefore,

$$|\psi^*\rangle = U^* |0\rangle^{\otimes n} \tag{F10}$$

is the unique ground state of H. Because unitary conjugation preserves the spectrum, the exact parent Hamiltonian retains the eigenvalues of H_0, including the zero ground-state energy and unit spectral gap.

3. Sparse Non-Clifford Parameter Sampling

Sampling every hidden rotation angle continuously can produce a large Pauli expansion after conjugation. To control this growth, we use a sampling procedure that combines Clifford rotations with a configurable number of non-Clifford rotations. Initially, each hidden angle is sampled from

$$\mathcal{C} = \left\{0, \frac{\pi}{2}, -\frac{\pi}{2}, \pi\right\}. \tag{F11}$$

A subset $\mathcal{S} \subseteq \{1, \ldots, p\}$ of size $|\mathcal{S}| = r$ is then selected. The corresponding angles are replaced by values sampled from $[-\pi, \pi)$, excluding Clifford-valued rotations. Thus, the hidden parameters follow

$$\theta_j^* \in \begin{cases} [-\pi, \pi) \setminus \mathcal{C}, & j \in \mathcal{S}, \\ \mathcal{C}, & j \notin \mathcal{S}, \end{cases} \tag{F12}$$

with angles understood modulo 2π. The parameter r controls the number of non-Clifford rotations in the hidden generating circuit. It does not restrict the optimization domain: all p parameters remain continuous and trainable. This distinction follows from the action of Clifford operations on Pauli operators. For any Clifford unitary C and Pauli string P,

$$CPC^\dagger = \pm P', \tag{F13}$$

where P' is another Pauli string. Consequently, Clifford conjugation does not increase the number of Pauli strings. In particular, when $r = 0$, the reference Hamiltonian is mapped to a sum of n nonidentity Pauli terms and one identity term. A non-Clifford Pauli rotation, by contrast, can split an anticommuting Pauli operator into two components. For example,

$$R_Y(\theta) Z R_Y^\dagger(\theta) = \cos(\theta) Z + \sin(\theta) X. \tag{F14}$$

Each non-Clifford rotation can therefore increase the term count by at most a factor of two. Before collecting repeated Pauli strings, the construction admits the bound

$$M \leq 1 + n2^r, \tag{F15}$$

where M includes the identity term. The actual number of nonzero terms may be considerably smaller because some Pauli strings commute with the applied rotations and repeated contributions can combine or cancel. The generated instances are also checked to avoid counting selected non-Clifford angles that have no effect on the resulting Hamiltonian. Thus, the sampling parameter r describes the intended non-Clifford content of accepted instances, rather than merely the number of continuous angles sampled.

4. Pauli Decomposition

The parent Hamiltonian is represented as

$$H = \sum_{j=1}^{M} c_j P_j, \qquad P_j \in \{I, X, Y, Z\}^{\otimes n}, \tag{F16}$$

with real coefficients c_j.

To obtain this representation, the reference Pauli terms are conjugated sequentially through the hidden circuit. For a gate of the form

$$R_P(\phi) = \exp\left(-i\frac{\phi}{2}P\right), \tag{F17}$$

where P is a Hermitian Pauli string, the conjugation of another Pauli string Q satisfies

$$R_P(\phi)QR_P^\dagger(\phi) = \begin{cases} Q, & [P,Q] = 0, \\ Q\cos\phi - iPQ\sin\phi, & \{P,Q\} = 0. \end{cases} \tag{F18}$$

This identity permits the Hamiltonian to be constructed using Pauli-string algebra, without explicitly forming a dense $2^n \times 2^n$ matrix. After combining identical strings, coefficients below a specified numerical tolerance are discarded. The resulting term count is evaluated against the prescribed budget K:

$$M \leq K. \tag{F19}$$

Instances are additionally subject to a maximum compiled native-gate depth $D_{\max}$:

$$D_{\text{native}} \leq D_{\max}. \tag{F20}$$

Candidate instances that do not satisfy the generation constraints are rejected, and new hidden parameters are sampled up to a specified attempt limit. These constraints control the size of the Hamiltonian representation and the circuit resources. They do not, by themselves, establish the computational difficulty of an accepted optimization problem.

5. Numerical Benchmark Configuration

The numerical benchmark spans three system sizes, $n \in \{4, 8, 12\}$, three entangling-layer counts, $L \in \{1, 2, 4\}$, and two non-Clifford rotation counts, $r \in \{1, 2\}$. For each combination, five instances are generated using seeds 42–46, resulting in $3 \times 3 \times 2 \times 5 = 90$ optimization problems. Table II summarizes these settings and the constraints imposed during generation.

For each candidate, the hidden angles are sampled according to Eq. (F12), the Pauli coefficients are constructed using Eq. (F18), and the resulting instance is checked against the term-count and compiled-depth limits. Candidates failing these constraints are rejected. The numerical coefficient cutoff and the native compilation basis are implementation-dependent settings and should be reported alongside the released generation code.

The resulting instances have known reference energies and exactly representable ground states, but they retain the structure of the circuit family used to generate them. They should not be interpreted as representative of arbitrary physical Hamiltonians. Moreover, neither the Pauli-term count nor the number of hidden non-Clifford rotations is, by itself, a measure of optimization difficulty. Classical optimization comparisons and additional structural analyses are reported in the following appendices.

Table II: Configuration of the random parent-Hamiltonian benchmark. The Pauli-term budget includes the identity contribution.

Setting	Value
Qubits n	$\{4, 8, 12\}$
Entangling layers L	$\{1, 2, 4\}$
Non-Clifford rotations r	$\{1, 2\}$
Random seeds	42-46
Trainable parameters p	$3n(L+1)$
Pauli-term budget K	16 ($r = 1$); 32 ($r = 2$)
Maximum compiled depth $D_{\max}$	100
Maximum generation attempts	250
Number of instances	90

Appendix G: Classical Optimization Comparisons

This appendix compares the language model optimizer (LMO) with classical optimization methods on the parent-Hamiltonian benchmarks defined in Appendix F. We compare the LMO with Adam as a conventional gradient-based reference, examining solution quality and the number of full-Hamiltonian expectation-value evaluations required.

1. Optimization Protocols and Resource Accounting

For each benchmark instance, the optimization objective is

$$E(\boldsymbol{\theta}) = \langle \psi(\boldsymbol{\theta}) | \, H \, | \psi(\boldsymbol{\theta}) \rangle \,, \tag{G1}$$

where the exact ground-state energy is $E_0 = 0$. All comparisons use exact, noiseless statevector simulations. A solution is considered successful when $E(\boldsymbol{\theta}) - E_0 \leq 10^{-6}$.

The LMO receives the parameterized circuit and its Pauli Hamiltonian as symbolic inputs. Its first parameter proposal is generated without previous objective evaluations. Subsequent proposals may incorporate the history of evaluated parameters and their energies. Each proposal specifies the complete parameter vector and is evaluated using the same Hamiltonian objective.

For comparison, we employ Adam with gradients computed through the parameter-shift rule. For a trainable parameter θ_j associated with a Pauli rotation,

$$\frac{\partial E}{\partial \theta_j} = \frac{1}{2} \left[E\left(\boldsymbol{\theta} + \frac{\pi}{2}\boldsymbol{e}_j\right) - E\left(\boldsymbol{\theta} - \frac{\pi}{2}\boldsymbol{e}_j\right) \right], \tag{G2}$$

where $\boldsymbol{e}_j$ denotes the corresponding coordinate vector. The ansatz contains $p = 3n(L+1)$ trainable parameters, so a direct gradient calculation requires $2p$ shifted full-Hamiltonian expectation evaluations. Additional evaluations of the unshifted objective are counted separately.

We report cumulative full-Hamiltonian energy evaluations rather than optimizer iterations alone. Each LMO proposal requires one evaluation to assess its energy, whereas each Adam update requires multiple evaluations to compute the gradient. The computational cost of language-model inference and other classical computations is not represented by this evaluation count.

The methods also use different information. The LMO receives the explicit circuit and Hamiltonian descriptions, whereas Adam accesses the objective through numerical energy and gradient evaluations. Accordingly, differences in objective-evaluation counts should not be interpreted as differences in total computational cost or as evidence of a general computational advantage.

Adam is evaluated for up to 200 optimization steps, the configurations are summarized in Table III.

2. Comparison with Adam

We compare LMO and Adam across configurations with $n \in \{4, 8, 12\}$ qubits, $L \in \{1, 2, 4\}$ entangling layers, and $r \in \{1, 2\}$ non-Clifford rotations in the generating circuit. Figures 10 and 11 present the optimization trajectories for the two benchmark families.

Table III: Optimization configurations used for the parent-Hamiltonian comparisons. All experiments use exact, noiseless energies.

Configuration	LMO	Adam
Parameter initialization	Model-generated	Seed 123
Initialization scale	–	0.3
Optimization rounds	Up to 5	200
Learning rate, $r = 1$	–	0.1
Learning rate, $r = 2$	–	0.01
Gradient method	None	Parameter shift
Shots per energy query	0	0
Noise	None	None

The vertical axis reports the best energy gap observed up to each recorded point,

$$\Delta E_{\mathrm{best}}(t) = \min_{s \le t} \left[E(\boldsymbol{\theta}_s) - E_0 \right]. \tag{G3}$$

The lower horizontal axis gives the cumulative number of full-Hamiltonian energy evaluations, while the upper axis indicates the corresponding Adam optimization iterations. For LMO, each recorded point corresponds to a complete parameter proposal evaluated using the Hamiltonian objective.

We can observe that in several configurations, Adam continues reducing the energy gap well beyond the initial iterations, eventually approaching the ground-state energy. In contrast, the LMO frequently reaches near-ground-state energies in its first proposal, without previous objective feedback. For these instances, the energy gaps are close to numerical precision after a single Hamiltonian evaluation. However, the LMO does not succeed universally, and some configurations exhibit substantially larger residual errors.

The comparison highlights the difference in Hamiltonian-evaluation requirements between the tested methods. Adam can obtain low-energy solutions through continued gradient-based optimization, whereas the LMO often produces suitable parameters before receiving objective feedback. These observations concern the specific structured benchmarks and optimizer configurations considered here, rather than a general comparison of computational efficiency. The parent Hamiltonian instances possess a planted structure that may be exploitable by specialized classical algorithms. The comparison with Adam therefore characterizes objective-evaluation requirements relative to a conventional gradient-based optimizer, rather than establishing classical hardness or a general computational advantage.

Appendix H: Structural Analysis of LMO Parameter Proposals

This appendix examines the structure of the parameter vectors generated by the language model optimizer (LMO) and the physical explanations accompanying its proposals. We investigate the role of non-Clifford rotations, the relationship between the proposed and generating parameter vectors, and the physical consistency of selected model-generated explanations.

1. Clifford-Angle Ablation and Parameter Non-Uniqueness

The parent-Hamiltonian instances are generated from parameter vectors containing predominantly Clifford-compatible angles, with either one or two non-Clifford rotations. To assess the contribution of continuous rotation angles to the LMO proposals, we perform an ablation in which every angle in the first proposal is replaced by its nearest Clifford-compatible value,

$$\widetilde{\theta}_j = \operatorname*{argmin}_{c \in \mathcal{C}} d_{2\pi}(\theta_j, c), \qquad \mathcal{C} = \{0, \pm\pi/2, \pi\}, \tag{H1}$$

where $d_{2\pi}$ denotes angular distance modulo 2π. The rounded parameter vectors are evaluated using the original Hamiltonians. Figure 12(a) compares the energy gaps before and after rounding. The original first proposals reach the success threshold of 10^{-6} in 40 of 45 instances for $r = 1$ and 37 of 45 instances for $r = 2$. After rounding, none of the 90 proposals satisfies this threshold. The median energy increase is approximately 0.052 for $r = 1$ and 0.109 for $r = 2$. Thus, although the proposed parameter vectors contain predominantly Clifford-compatible angles, rounding all angles to this discrete set substantially reduces their accuracy. We also investigate whether successful proposals

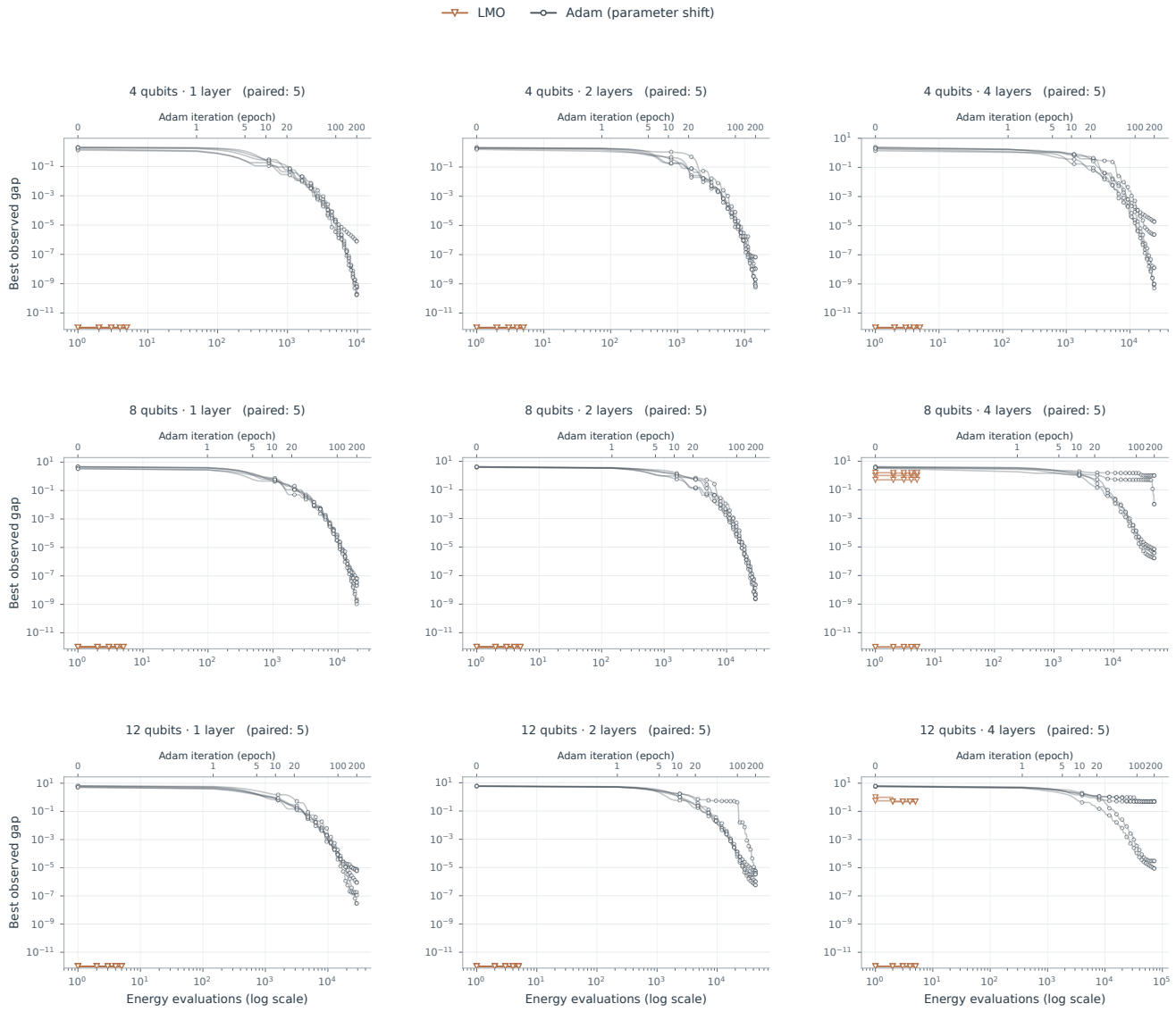


Figure 10: Optimization trajectories for parent Hamiltonians with $r = 1$ non-Clifford rotation in the generating circuit. Each panel corresponds to a configuration of qubit count and entangling layers and includes the available paired instances. The curves show the best-observed energy gaps against cumulative full-Hamiltonian evaluations. The upper axis indicates Adam iterations.

recover the hidden parameter vectors used to construct the parent Hamiltonians. For each first proposal, we compute the wrapped Euclidean distance from the generating parameters,

$$d_\theta = \left[\sum_{j=1}^{p} \mathrm{wrap}_{2\pi}(\theta_j - \theta_j^*)^2 \right]^{1/2}, \tag{H2}$$

and the fidelity with the exact ground state,

$$F = |\langle \psi^* | \psi(\boldsymbol{\theta}) \rangle|^2 . \tag{H3}$$

The hidden generating parameters are used only for this post-hoc analysis and are never provided to the LMO. Figure 12(b) shows the ground-state infidelity as a function of parameter distance. The median wrapped distances

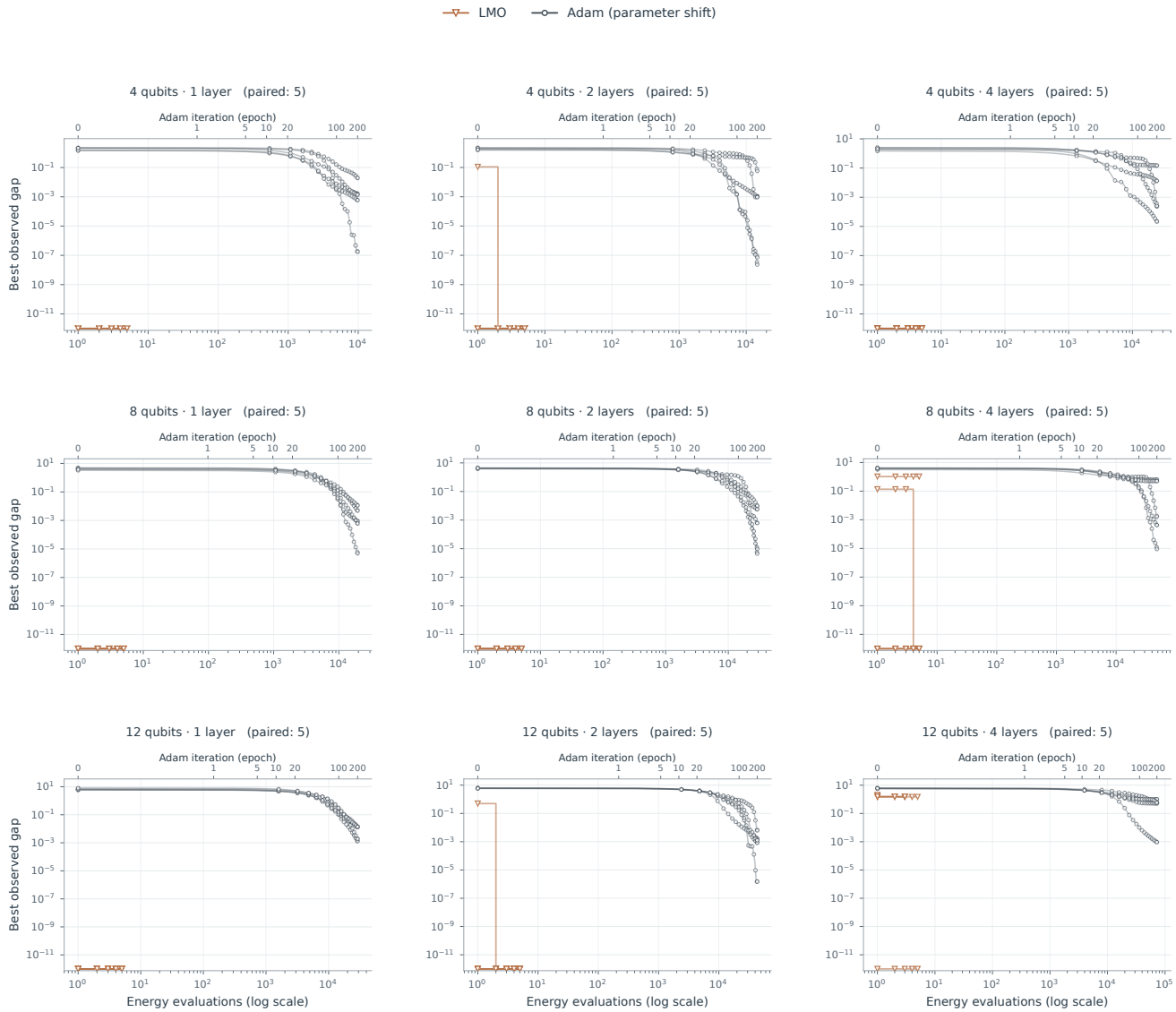
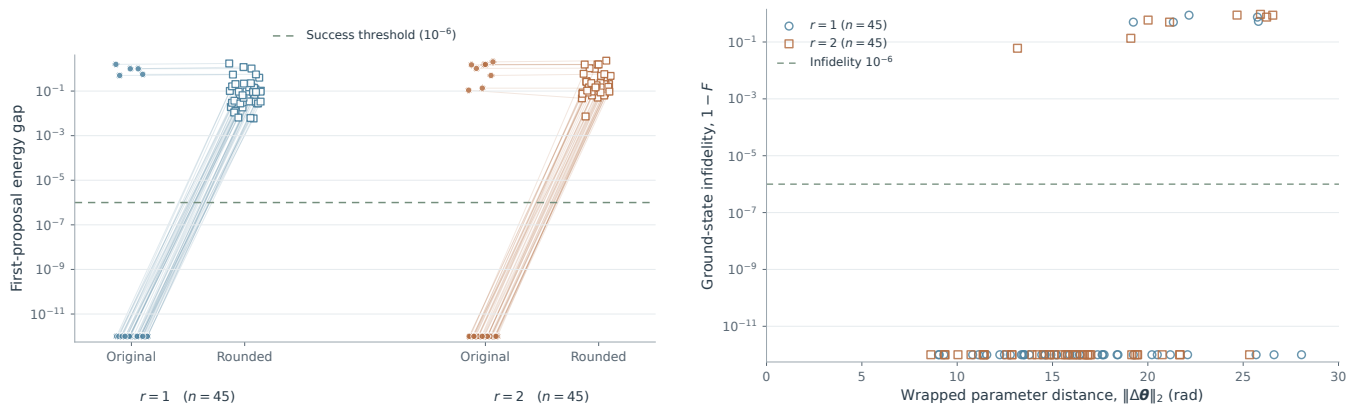


Figure 11: Optimization trajectories for parent Hamiltonians with $r = 2$ non-Clifford rotations in the generating circuit. The plotting conventions are the same as in Fig. 10.

are approximately 15.90 and 16.18 radians for $r = 1$ and $r = 2$, respectively, despite median ground-state fidelities close to unity. Furthermore, the complete sets of non-Clifford parameter positions match those of the generating circuits in only three instances for $r = 1$ and two for $r = 2$. These results indicate that successful ground-state preparation does not generally require recovery of the generating parameters. Distinct parameter vectors can prepare the same state without implementing identical unitaries on arbitrary inputs. Moreover, the rounding ablation evaluates the simultaneous replacement of all angles; it does not establish that each individual non-Clifford rotation is necessary.

2. Analysis of LMO-Proposed Mechanisms

In addition to a parameter vector, the LMO generates a textual explanation describing a possible physical mechanism underlying its proposal. We examine these explanations to characterize their physical content and assess the consistency of selected claims with independent numerical calculations.



(a) (b)

Figure 12: Structural analysis of the first LMO proposals for random parent Hamiltonians. (a) Energy gaps before and after rounding the proposed angles to Clifford-compatible values. The dashed line indicates the success threshold of 10^{-6}. (b) Ground-state infidelity versus wrapped Euclidean distance from the hidden generating parameters. Small infidelities can occur despite large parameter distances, illustrating the non-uniqueness of successful state-preparation parameters.

We analyze the explanations accompanying the first proposals for all 90 parent-Hamiltonian instances. Every proposal includes a nonempty explanation, with median lengths of 42 words for $r = 1$ and 44 words for $r = 2$. Automated textual annotations identify references to specific Pauli operators in 39 explanations, correlation-related language in 42, and energy-related language in 86. These counts describe textual content and do not constitute assessments of physical correctness.

The explanations include proposed strategies based on Pauli eigenstate preparation, alignment of local rotations with Hamiltonian terms, and the use of entangling gates to establish quantum correlations. Such statements can contain testable claims about intermediate states, Pauli expectation values, or the resulting energy. We illustrate their physical consistency using two contrasting first-proposal examples, shown in Figure 13.

In the first example, the LMO proposes preparing X-eigenstates such that the fixed R_{XX} gates act only through phases, followed by a local rotation aligning a qubit with an effective Hamiltonian field. The checked state-preparation and field-alignment claims are consistent with the proposed parameters, and the resulting energy gap is approximately zero. In the second example, the LMO states that its proposed parameters satisfy all 12 commuting parent-Hamiltonian constraints, predicting zero energy. Independent evaluation, however, yields an energy gap of 0.5 and ground-state fidelity of approximately 0.5, contradicting that prediction.

These examples illustrate that model-generated explanations can contain physically verifiable claims, but their correctness is not guaranteed. The two cases are selected to demonstrate contrasting outcomes and do not provide an estimate of explanatory correctness across the full benchmark. Furthermore, agreement between an explanation and independent calculations does not establish that the explanation faithfully represents the model's internal decision process. Parameter-generation performance and explanatory correctness are therefore treated as distinct properties.

Appendix I: Circuit Interpretability: Experimental Protocol and Additional Analysis

This appendix provides additional details on the circuit construction, representation transformations, and evaluation protocol used in the blind circuit-interpretation experiments. We distinguish the recognition of an algorithmic family from the prediction of its computational behavior and the physical consistency of the accompanying explanations.

1. Circuit Construction and Representation Transformations

We consider three algorithmic families: Grover's search, the quantum Fourier transform (QFT), and Bernstein-Vazirani. Five instances are generated for each family, with different problem parameters or input states. Each instance is represented in logical, native, and obfuscated forms, resulting in 45 circuit descriptions. For Grover's search, we use three search qubits and two Grover iterations, with five distinct marked bitstrings. The resulting

(a) Physically supported proposal $n = 4$, $L = 1$, $r = 1$, **seed 42**

```
"theta":  [24 values omitted]

"mechanism":

Initialize all qubits in +X, making both RXX gates global phases.  Final rotations
align q0 opposite (0.4598856, 0.1962276, 0), retain q1 and q2 in +X, and put q3 in +Z.
This attains the Hamiltonian lower bound, approximately zero.
```

Independent verification. $\langle X_0 \rangle = -0.919771$, $\langle Y_0 \rangle = -0.392455$, and $\Delta E \simeq 0$. The checked physical claims are supported.

(b) Contradicted proposal $n = 12$, $L = 2$, $r = 2$, **seed 42**

```
"theta":  [108 values omitted]

"mechanism":

Constructs a locally rotated stabilizer state satisfying all 12 commuting Hamiltonian
constraints.  The non-Clifford rotations on q2 and q7 match the two weighted Pauli
pairs.  Predicted expectation is zero up to numerical precision.
```

Independent verification. $\Delta E = 0.5$ and $F \simeq 0.5$. The zero-energy prediction is contradicted.

Figure 13: Contrasting examples of LMO-generated physical explanations for parent-Hamiltonian optimization. (a) A successful proposal whose checked physical claims are consistent with independent numerical verification. (b) A proposal whose predicted zero-energy state is contradicted by independent evaluation. The JSON-style excerpts are abridged for presentation: parameter arrays are omitted and long text is line-wrapped.

measurement distribution favors the marked state but is not deterministic. For Bernstein-Vazirani, we use four input qubits and one ancilla, with five distinct nonzero secret bitstrings. The circuit implements a binary parity oracle, and the measured input register returns the corresponding secret in the ideal setting. For QFT, we consider four-qubit circuits with five independently generated product-state inputs. Each input is prepared using single-qubit R_Y and R_Z rotations, followed by the QFT and computational-basis measurements. These input states provide distinct measurement distributions and allow the numerical behavior of each circuit to be evaluated independently.

The logical representation uses standard quantum gates, with algorithm-specific identifiers and comments removed. The native representation is obtained by transpiling the same circuit into the restricted gate set

$$\mathcal{G}_{\text{native}} = \{R_Z, R, R_{XX}\}, \tag{I1}$$

where R denotes the parameterized single-qubit rotation supported by the chosen compilation basis. The native representation preserves the implemented computation while replacing familiar high-level gate sequences with lower-level operations.

To further modify the circuit representation, we introduce randomized local Clifford frames between groups of logical gates. Let the original unitary be decomposed into m consecutive blocks,

$$U = G_m G_{m-1} \cdots G_1. \tag{I2}$$

We sample local Clifford transformations $C_1, \ldots, C_{m-1}$, with boundary conditions $C_0 = C_m = I$, and define

$$\widetilde{G}_i = C_i G_i C_{i-1}^{\dagger}. \tag{I3}$$

The transformed circuit satisfies

$$\widetilde{U} = \widetilde{G}_m \cdots \widetilde{G}_1 = G_m \cdots G_1 = U, \tag{I4}$$

because the intermediate frame transformations cancel between consecutive blocks. In our implementation, frames are sampled from tensor products of single-qubit Clifford gates, with transformations introduced between groups of four logical operations. Each transformed block is independently compiled into $\mathcal{G}_{\text{native}}$. This blockwise compilation

avoids applying a final global optimization that could eliminate many of the inserted frame transformations. The procedure changes the gate-level description without changing the implemented unitary.

The logical, native, and obfuscated representations are generated from the same underlying instance. Only the resulting OpenQASM 3 description is provided to the LLM. The original circuit, transformation metadata, expected outcomes, and equivalence checks are excluded from the inference prompt. The randomized-frame construction is used as a controlled representation transformation rather than a cryptographic obfuscation method. In particular, the transformed circuits may contain additional gates and longer descriptions, and their structure may remain recoverable through suitable circuit simplification.

2. Interpretation Prompt and Evaluation Protocol

All circuit interpretations are generated using the same frozen language model and fixed system instructions. The model receives only the anonymized OpenQASM 3 description of an instantiated circuit and is instructed to analyze its operations without using external tools, simulations, or experimental feedback. The requested response is a structured JSON object containing a description of the circuit's mathematical behavior, a hypothesis about its computational purpose, predicted measurement behavior, supporting gate-level evidence, alternative interpretations, properties that cannot be identified, and a confidence value associated with the algorithm hypothesis. The inference protocol also permits explicit predictions of the most likely output bitstring and, when feasible, a measurement probability distribution. The model may abstain from these numerical predictions when they cannot be reliably inferred. No ground-truth information is provided during inference, and all interpretations are generated without feedback from previous circuit evaluations.

We distinguish three aspects of the generated interpretations. First, algorithm identification evaluates whether the reported algorithm hypothesis matches the known circuit family. This criterion measures recognition of the algorithmic structure but does not establish correctness of the predicted computation. Second, functional output prediction evaluates the explicit numerical predictions against independently calculated outcomes. For Grover and Bernstein-Vazirani, we compare the predicted most-likely bitstring with the exact most-likely measurement outcome. A correct prediction receives a score of one; an incorrect or absent prediction receives zero when calculating accuracy over all valid responses. Third, physical explanation consistency concerns the supporting claims produced by the model. These may describe the roles of specific gates, interference, phase accumulation, or the relationship between the circuit structure and its computational output. Such explanations are evaluated separately from algorithm identification and numerical output prediction.

3. Additional Analysis of Model-Generated Interpretations

The complete benchmark contains 45 valid interpretations, with five instances for each combination of algorithm and circuit representation. All three representations are evaluated independently, allowing algorithm identification and functional prediction to be compared for the same underlying computations. The results reveal a distinction between algorithm identification and numerical output prediction. In the logical representation, the model identifies all 15 algorithmic instances. Under native decomposition and obfuscation, the corresponding totals are 11 and 12 correct identifications, respectively.

This distinction is particularly pronounced for Bernstein-Vazirani. Although the model identifies the algorithm in only two of five native and two of five obfuscated instances, it predicts the correct secret bitstring in all ten. Thus, the numerical output can remain correct even when the conventional algorithmic label is not recovered. For Grover's algorithm, the model correctly predicts the most likely output in five logical, four native, and five obfuscated instances. For QFT, the algorithm is identified in all 15 cases. However, these identification results alone do not determine whether the model's explanations correctly describe the underlying quantum transformations.

The transformations also modify circuit depth and OpenQASM description length. Consequently, differences across representations may reflect both changes in recognizable gate patterns and the additional complexity of the circuit descriptions. The experiment does not isolate these effects or establish that the model's interpretations are independent of previously learned algorithmic patterns. Nevertheless, the results demonstrate that algorithm identification and functional output prediction need not vary together under equivalent circuit representations. This distinction motivates evaluating the mathematical behavior inferred by a language model separately from its ability to recognize familiar quantum algorithm structures.

Boxes 1 and 2 present the complete LLM responses for two equivalent representations of the same Bernstein–Vazirani instance. In the logical representation, the model identifies Bernstein–Vazirani as its most plausible interpretation and correctly predicts the output bitstring 0100. In the obfuscated representation, the model does not identify a unique

algorithmic purpose but still predicts the same output, illustrating the distinction between algorithm identification and functional prediction.

(a) Logical representation


```
{
  "circuit_behavior": "The circuit prepares q[0] through q[3] in |+> and q[4] in |->. The CNOT implements the oracle f(x)=x[2].
     Because X|->=-|->, it introduces the phase (-1)^x[2] without entangling the ancilla with the input register. The final
     Hadamards leave q[0], q[1], and q[3] in |0>, and q[2] in |1>. The unmeasured ancilla remains in |->.",
  "algorithm_hypothesis": "Bernstein\u2013Vazirani with hidden string 0100 is the best-fitting interpretation, but the intended task
      is ambiguous.",
  "predicted_measurement_behavior": "In ideal execution, the measurements always give c[3]=0, c[2]=1, c[1]=0, and c[0]=0.",
  "predicted_most_likely_bitstring": "0100",
  "predicted_probabilities": {
    "0100": 1.0
  },
  "evidence": [
    "The X followed by H on q[4] prepares the phase-kickback ancilla |->.",
    "Initial Hadamards prepare an equal superposition of all 16 input-register basis states.",
    "The only oracle gate is cx q[2], q[4], corresponding to the linear Boolean function f(x)=x[2].",
    "Phase kickback changes q[2] from |+> to |->; the final Hadamard maps it to |1>.",
    "On q[0], q[1], and q[3], the two Hadamards cancel, leaving |0>.",
    "The measurement mapping places the sole 1 in c[2], giving 0100 in descending classical-bit order."
  ],
  "alternative_hypotheses": [
    "A Deutsch\u2013Jozsa circuit for the balanced function f(x)=x[2]; its nonzero output certifies the balanced case under the
      usual promise.",
    "A demonstration of phase kickback or Hadamard-basis interference without an intended oracle-identification task."
  ],
  "not_identifiable": [
    "Whether the intended task is hidden-string recovery, constant-versus-balanced classification, or a gate-level demonstration.",
    "Whether the oracle is intended to be unknown to an executing algorithm.",
    "Physical noise rates and actual hardware outcome frequencies."
  ],
  "confidence": 0.85
}
```


Independent verification. Exact most-likely output: `0100` ($P = 1$). The model identifies Bernstein-Vazirani as its preferred interpretation.

(b) Obfuscated representation


```
{
  "circuit_behavior": "Starting from all-zero qubits, the circuit produces |0> on q[0], |0> on q[1], |1> on q[2], |0> on q[3], and
     |-> on q[4], up to an overall phase. The sole two-qubit interaction does not entangle this input: immediately before it, q[2]
     is |1> and q[4] is the X eigenstate |->. Consequently, rxx(pi/2) acts as Rx(-pi/2) on q[2]. Subsequent rotations restore q[2]
     to |1> and leave q[4] in |-> up to phase.",
  "algorithm_hypothesis": "not identifiable",
  "predicted_measurement_behavior": "In ideal execution, every shot returns c[3]=0, c[2]=1, c[1]=0, c[0]=0. The unmeasured fifth
     qubit does not introduce randomness into these results.",
  "predicted_most_likely_bitstring": "0100",
  "predicted_probabilities": {
    "0100": 1.0
  },
  "evidence": [
    "The custom gate r(theta, phi) equals exp[-i theta (cos(phi) X + sin(phi) Y)/2]. Thus r(theta, 0)=Rx(theta) and r(theta, pi/2)=
     Ry(theta).",
    "A chronological pair Ry(pi/2), Rx(pi) implements -iH. On q[0], four such pairs and two additional Rx(pi) gates reduce to
     identity up to phase. On q[1], four such pairs also reduce to identity.",
    "On q[3], two such pairs followed by two Rz(pi) rotations reduce to identity up to phase.",
    "Before rxx, the opposite Rz(pi/2) rotations on q[2] cancel, as do its two adjacent Rz(pi) rotations up to phase. Its remaining
     Ry(pi/2), Rx(pi), Ry(pi/2) sequence equals Rx(pi), preparing |1>.",
    "Before rxx, the Rz(pi) rotations on q[4] cancel in pairs up to phase. Its remaining Rx(pi), Ry(pi/2), Rx(pi) sequence prepares
     |-> up to phase.",
    "The supplied rxx decomposition implements exp[-i theta X\u2297X/2]. Since X|->=-|->, its action here is Rx(-pi/2) on q[2].",
    "After rxx, the opposite Y rotations on q[2] cancel. Combining the interaction's effective Rx(-pi/2), the explicit Rx(-pi/2),
     and the final Rx(pi) gives identity. The final Rx(-pi/2) on q[4] contributes only a phase."
  ],
  "alternative_hypotheses": [
    "A deterministic state-preparation circuit containing redundant rotations.",
    "A gate-rewriting or compilation test whose intended significance is not visible in its final measurement statistics."
  ],
  "not_identifiable": [
    "A unique named algorithm or intended computational problem.",
    "Whether the redundant gates are intentional, compiler-generated, or part of a larger omitted computation."
  ],
  "confidence": 0.1
}
```


Independent verification. Exact most-likely output: `0100` ($P = 1$). The model does not identify a unique algorithmic purpose.